

PARTICLES IN THE PACIFIC: HOW PRODUCTIVITY AND ZOOPLANKTON
RELATE TO PARTICLES IN THE DEEP SEA

By

Jessica L. Pretty, B.S. Ocean and Earth Science

A Thesis Submitted in Partial Fulfillment of the Requirements

for the Degree of

Master of Science

in

Oceanography

University of Alaska Fairbanks

May 2019

APPROVED:

Andrew McDonnell, Committee Chair

Mark Johnson, Committee Member

Russ Hopcroft, Committee Member

Mark Johnson, Chair

Department of Oceanography

Bradley Moran, Dean

College of Fisheries & Ocean Sciences

Michael Castellini

Dean of the Graduate School

Abstract

The magnitude and spatio-temporal patterns of particulate material flux from the surface ocean through mesopelagic and bathypelagic depths determines sequestration of atmospheric carbon and the food supplied to deep-dwelling ocean life. The factors that influence how and where this organic material is exported from euphotic depths are poorly understood. Zooplankton are thought to play a key role in modulating the transport of surface-produced particles to depths through consumption, fragmentation, active diel vertical migration, and fecal pellet production, thus it is important to study both particulate matter and zooplankton in tandem. In this study, I use an *in-situ* optical instrument, the Underwater Video Profiler 5 (UVP5), to describe broad scale patterns of large ($> 100 \mu\text{m}$) particles and zooplankton across a longitudinal transect of the Pacific Ocean during April to June 2015. Satellite-derived surface chlorophyll-a was employed to describe the timescales over which particles arrive in meso- and bathypelagic depths after a productivity peak. High abundances and volumes of particles are noticeable beyond the euphotic zone across the Equator, transition zone, and the sub-arctic Pacific, indicating increased export in these high-nutrient low-chlorophyll (HNLC) areas. In two of these areas, the Equator and transition zone, large abundances and volumes of particles extend into bathypelagic depths. High abundances of zooplankton were seen in all areas where high abundances of particles are seen in bathypelagic waters. Rhizaria were revealed to be pervasive across all biogeographic regions, and appear to play a role in particle attenuation in the sub-arctic Pacific. The insight into patterns between particles, zooplankton, and productivity identify HNLC regions as deserving more detailed examination in future studies of biological pump efficiency.

Table of Contents

Abstract.....	ii
List of Figures.....	iv
List of Tables.....	iv
Acknowledgements.....	v
Introduction.....	1
Methods.....	11
Study Area and Sampling Strategy.....	11
Data Collection and Processing.....	13
Image Sorting.....	14
Using Data from Ecotaxa Database.....	16
Calculation of Zooplankton Abundance.....	17
Satellite- Derived Chlorophyll-a.....	17
Results.....	18
Patterns in Particle Abundance, Size, Volume, and PSD.....	18
Patterns in Satellite-derived Surface Chlorophyll-a.....	21
Patterns in Zooplankton Distribution and Abundance.....	22
Discussion.....	26
Patterns in Particles Across the Pacific.....	26
Patterns in Zooplankton Across the Pacific.....	27
Connecting Particles and Zooplankton.....	31
Conclusions.....	33

References.....	35
Appendix.....	41

List of Figures

Figure 1. Biological pump schematic	4
Figure 2. Station Map of P16N CLIVAR repeat hydrography cruise	12
Figure 3. Examples of zooplankton images captured by the UVP5	15
Figure 4. Total particle abundance.....	19
Figure 5. Microscopic particle (0.161-0.203 mm) abundance (#/L).....	19
Figure 6. Macroscopic particle (0.203-2.58 mm) abundance (#/L).....	20
Figure 7. Mean size (mm) of particles	20
Figure 8. Particle volume ($\text{mm}^3 \text{L}^{-1}$).....	21
Figure 9. Surface Chlorophyll-a with cruise track.....	22
Figure 10. Zooplankton abundance ($\#/m^3$)	23
Figure 11. Zooplankton community composition.....	24
Figure 12. Abundance of zooplankton taxa	25

List of Tables

Table 1. Comparison of zooplankton abundances between UVP and net tows.....	30
---	----

Acknowledgements

First I want to thank my advisor, Andrew McDonnell, for accepting me as student and being particularly patient with me, as I navigated through this degree. I'd also like to thank my committee members, Russ Hopcroft and Mark Johnson, for your guidance through courses as well as extensive help through the thesis writing process.

I would like to thank the crew of the NOAA Vessel *Ronald Brown* and scientists during the P16N CLIVAR Cruise in 2015 for supporting and the data collection necessary for this research. Particular thanks goes to both Jessie Turner and Andrew McDonnell who ran the UVP on each leg of the P16N CLIVAR cruise. In addition I'd like to thank the crew and other scientists aboard the *R/V Sikuliaq* in Spring of 2018 for making even the roughest days at sea enjoyable in the Gulf of Alaska. Additional thanks the Hopcroft and Coyle labs for sharing access to the zooplankton net-tow data. Profuse thanks also goes to Marc Picheral and his coworkers in Villefranche, France for answering endless questions at all hours about the UVP and the Ecotaxa database.

Much thanks to NSF for funding support through many grants (OCE #: 1421118, 145983, 1654663) and NASA EXPORTS for funding much of my time as a graduate student and M.J. Murdock Charitable Trust for equipment purchase assistance. I am also extremely grateful to UAF, the College of Fisheries and Ocean Sciences, and Brenda Konar for additional funding through teaching assistantships. Endless amounts of thanks to all the friends and fellow graduate students who helped me through this process, especially Ali, Cat, Ann, Katie, Beka, Faith, Robbie, Liza, and Brian. Last, but certainly not least, I'd like to thank my parents, step-parents, grandparents, and Andy Parke, whose tireless support and belief in me mean more than I can ever hope to expres

Introduction

Increasingly, one of the tasks of oceanographers is to predict the impact of climate change on marine ecosystems and these systems' ability to regulate increasing atmospheric carbon dioxide (CO₂). The ocean has, and will, continue to serve as a reservoir for carbon over long time scales, from hundreds to thousands of years. Carbon's fates are determined by the vertical flux of both dissolved and particulate material by both physical and biological pumps (Sarmiento and Gruber 2006). The physical carbon pump refers to the movement of dissolved inorganic carbon (DIC) from the surface to the interior of the ocean via physical movement of water parcels. The biological pump encompasses the set of processes by which DIC in surface waters is transformed by photosynthesis into particulate organic carbon (POC) and dissolved organic carbon (DOC), both of which have a variety of fates. A portion of this organic matter is transported out of the euphotic zone in the form of particles to deeper layers of the ocean and an even smaller amount eventually reaches the ocean floor. Carbon exported to depth from the euphotic zone is considered sequestered, at least until it cycles back to the surface. These pumps facilitate the ocean's role as a long-term 'storage-unit' for CO₂, helping mitigate changes in atmospheric CO₂ (Sarmiento and Le Quéré 1996). It is estimated that without the influence of the ocean's biological pump, the concentration of CO₂ in the atmosphere would be at least 150ppm higher than current levels (Sarmiento and Toggweiler 1984; Maier-reimer et al. 1996).

Carbon in the form of particles can move quickly through the water column allowing for storage in deep waters. The term particle vaguely describes anything that can be trapped on a filter or mesh, spanning sizes from about 0.02µm to centimeters in

diameter. This description encompasses both living organisms (i.e., zooplankton, phytoplankton, bacteria and archaea) and non-living organic matter (i.e., marine snow and detritus), as well as lithogenic matter and other inorganic minerals (Stemmann and Boss 2012a).

For society to prepare for the changes in the carbon cycle ahead, it is imperative to understand the mechanisms responsible for variation in both the physical and biological pumps so as to quantify the ocean's uptake and storage of carbon. The variation in the strength of the two pumps arises due to the differences in both physical dynamics, such as temperature and mixing, as well as biological dynamics, such as primary production and heterotrophic activity. Concerns about climate change are motivating multinational investigations into the carbon cycle including, most recently (in 2018), the NASA-funded 'Export Processes in the Ocean from RemoTe Sensing' (EXPORTS) to "develop a predictive understanding of the export and fate of global ocean net primary production and its implication(s)" (Siegel et al. 2016).

Constraining both the physical and biological pumps is a complex undertaking. The physical carbon pump is a transport mechanism relying on the solubility of gases in seawater: gases are more soluble at lower temperatures and under greater pressure, resulting in the deep ocean acting as a large storage compartment for CO₂. Comparisons among models of the physical carbon pump suggest that the major difference in CO₂ sequestration estimates is related to how deep-water formation is handled within each model (Toggweiler et al. 2003). Models of the biological pump are more poorly constrained than those of the physical pump. The fate of material generated by primary production in surface waters is impacted by higher trophic levels, aggregation and

fragmentation processes, as well as remineralization. Transport of material out of the surface ocean by the biological pump consists of three main mechanisms: passive sinking of POC, transport by animals including zooplankton, and mixing of dissolved organic matter (Volk and Hoffert 1985). Aggregation and fragmentation of particles are important components of the numerous and interrelated processes which influence the rate at which material sinks (De La Rocha and Passow 2007). These sinking rates are estimated using Stokes' Law, which predicts that larger and denser particles sink faster than smaller, less dense particles. The speed at which particles sink is of fundamental importance because the majority of remineralization of POC and other biological interactions with particles occur in the top 1000 meters of the ocean (Martin et al. 1987; Burd and Jackson 2009). The faster particles sink through these depths, the lower the chances of their remineralization and fragmentation into DIC and DOC, and the greater their probability of long term carbon storage.

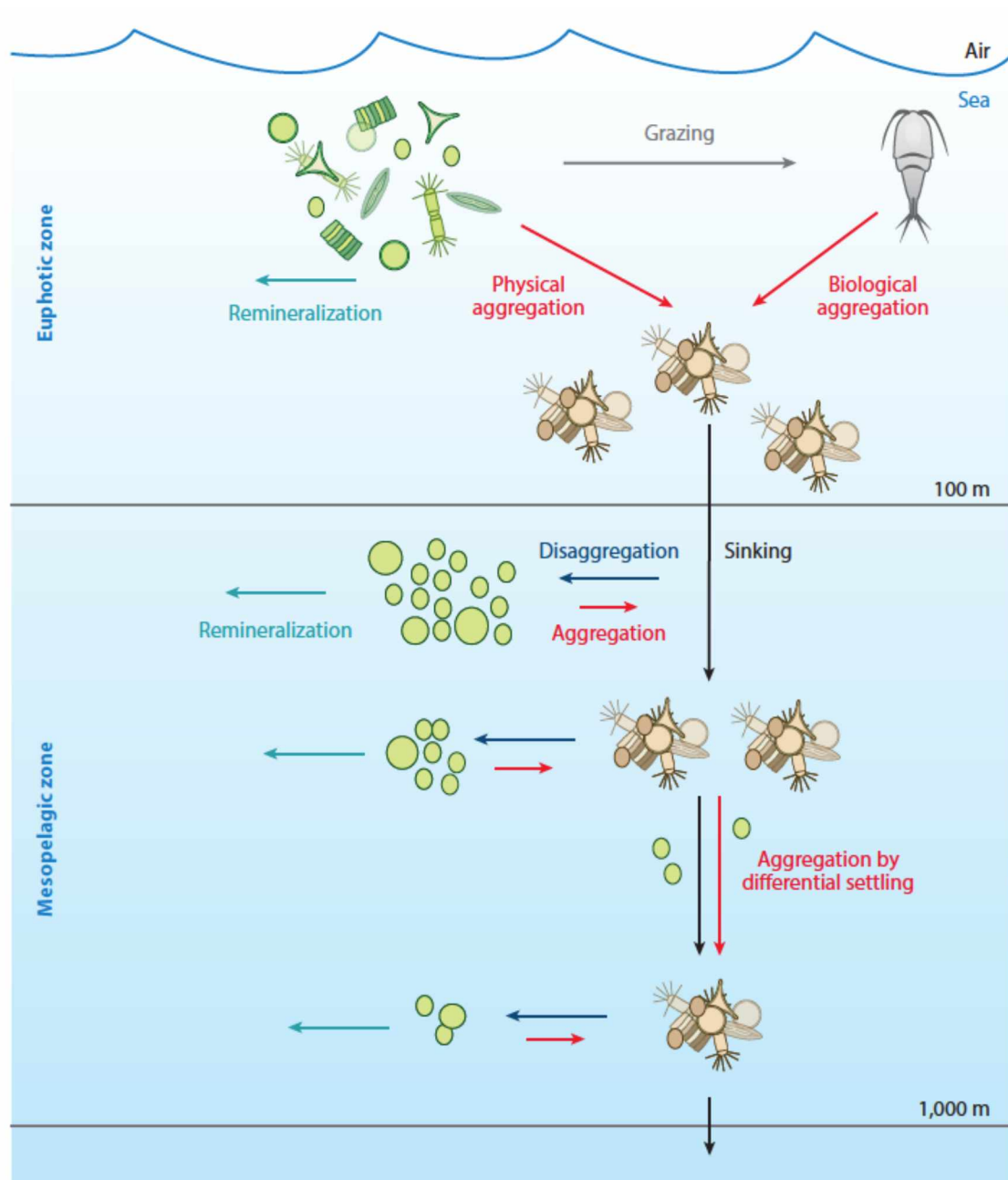


Figure 1. Biological pump schematic. A simplified depiction of the biological carbon pump. Red arrows indicate aggregation, dark blue arrows indicate disaggregation, light blue arrows remineralization from POC to DOC, and black arrows indicate sinking. Suspended material, shown in green, includes small phytoplankton, particles produced locally, and non-sinking lithogenic particles. Sinking aggregates are shown in brown, and comprise of phytoplankton, fecal pellets, and lithogenic ballasting material. [From Lam & Marchal 2015]

Unfortunately, it is difficult – if not impossible – to pinpoint the biologically-influenced particle transformation processes such as sloppy feeding (disaggregation) or fecal pellet production (aggregation) by zooplankton. To better understand these transformation processes, efforts have focused on either regionalizing the parameterization of export processes (e.g. Boyd and Trull 2007) or describing the distribution of particles and zooplankton, both vertically throughout the water column and spatially across large distances (e.g. Jackson et al. 1997; Guidi et al. 2008). With filtration techniques and sediment trap collection, particles are examined in the laboratory by sizing particles, classifying type (by morphology or source), and finding chemical composition in addition to their concentration. Optical instruments have the advantage of quick size analysis, but lack composition data without further effort. Comparisons of biogeochemical models attempting to constrain the biological pump using the size and composition of particles have also highlighted the importance of aggregation processes that increase particle size, as well as the composition of the zooplankton community, although the specific role of each zooplankton taxa remains elusive (Stemmann et al. 2004a; Gehlen et al. 2006).

Due to the complexity of interactions between zooplankton and particles, studies that couple the analysis of both, along with other physical and biological data, are essential to describe the influence of zooplankton on particle export. Zooplankton transfer carbon and other elements from surface waters to depth in two main ways: passively through fecal pellets sinking and actively when vertically migrating animals release carbon that was originally ingested in shallower waters into deep waters via respiration and excretion/defecation. In addition, the forces exerted by the swimming motion of

zooplankton can also affect the particulate matter they pass that is otherwise passively sinking. For example, the swimming action of euphausiids can fragment particles passing within 8-10 mm of them, thereby increasing the number of particles and decreasing particle size along the pathway of their daily vertical migration (Dilling and Alldredge 2000). Presumably, the diel migrations by other zooplankton also have the potential to tear apart larger particles and therefore slow down their sinking rate.

Different ingestion mechanisms by zooplankton also have varying effects on the size of particles, which in turn impact the flux of material. Ingestion mechanisms are broadly described by zooplankton taxa. Predatory zooplankton, including chaetognaths and some crustaceans, target other plankton and particles and tend to engulf their prey, removing these large particles from the water column and driving down the mean size of particles present. Filter-feeders, such as suspension-feeding copepods, pteropods, and larvaceans, coagulate small particles and repackage them into larger parcels. Larvaceans and pteropods produce large mucus structures, collecting small particles into a larger mass during filtration. These structures are sometimes discarded, and end up making up a significant portion of large marine particles known as ‘marine snow’ (Alldredge 2005). Copepods and other zooplankton that actively ‘sweep’ the water column using comb-like appendages are able to tease out small particles from the water column before ingestion, repackaging and egestion of material as fecal pellets. In food-rich environments, many of these fecal pellets can contain densely packed, poorly-digested particulate organic matter that is able to sink quickly once egested.

Fecal pellets make up significant portions of the total flux of POC to depth in different regions, though their source and magnitude are highly variable. Copepods and

euphausiids produce fecal pellets that have high sinking rates, but while they typically dominate zooplankton communities, their fecal pellets' contribution to export and sequestration flux is highly variable and dependent on the type and concentration of food present (Turner 2002). Pelagic tunicates have been shown to contribute substantially to pellet flux when they are abundant (Madin et al. 1982, Gorksy and Fenaux 1998). Similarly, pteropods create a large mucus structure that is reingested, then later released in pellet form, with their pellets contributing as much as 10-30% of the total POC flux to 180 m annually in Terra Nova Bay, Ross Sea (Manno et al. 2010). Even fecal pellets from chaetognaths can contribute up to 12% of total vertical carbon flux to 360 m depth in the Lazarev Sea (Giesecke et al. 2010). Phaeodarians, a member of the large protist Rhizaria taxa, have recently been able to intercept > 20% of sinking particles before they reach a depth of 300 m in the California Current system (Stukel et al. 2018). These examples reinforce the idea that zooplankton community composition plays a key role in particle export.

The biological pump is described as varying in both magnitude (strength) and remineralization length scale (transfer efficiency) of POC flux (Lam and Marchal 2015). Multiple approaches have been taken to estimate both the strength and transfer efficiency. Until recently, most of the decrease in particle flux through mesopelagic depths was estimated using a single parameterization of POC flux vs depth (Martin et al. 1987), or quantification and examination of particles from sediment traps deployed at depths beyond 1000 meters (Honjo et al. 2008). Currently, sinking particles are studied in various ways, including in situ bottle collection or pumping (Trull and Armand 2001; Savoye et al. 2008), sediment traps (Honjo et al. 1987; von Bodungen et al. 1995), optical

instruments (McDonnell and Buesseler 2012), and combinations of these methods (Guidi et al. 2008; McDonnell and Buesseler 2010). Each method has different strengths and weaknesses to be balanced or combined to reach desired research goals (McDonnell et al. 2015). Chemical measurements on particles, such as the disequilibrium of ^{234}Th relative to its parent ^{238}U , are used for estimating export fluxes. Buesseler and Boyd (2009) introduced new useful parameters to describe POC flux out of the euphotic zone relative to net primary production (Ez-ratio) and the ratio of flux of POC 100m below the depth of the euphotic zone (Ez) to POC flux at Ez (T_{100}). These terms have helped to characterize the spatial and temporal patterns of surface export and subsurface flux attenuation, however, different methods result in often contradictory evidence. Satellite data (chlorophyll and sea surface temperature) combined with algorithms developed from deep-moored sediment traps and flux derived from ^{234}Th disequilibria data suggest that attenuation of particles happens most rapidly in cold waters at high latitudes (Henson et al. 2012). In contrast, Marsay et al (2014), combined deep sediment trap fluxes from neutrally-buoyant sediment traps (NBSTs) with climatological satellite temperature data and found that colder waters and higher latitudes correlate with increased transport efficiency and slower attenuation of particles with depth (See Figure 3 in Marsay et al. 2014). Although rationale has been suggested to resolve this apparent disagreement, the prevalence of contradictory evidence about POC flux highlights the need for larger scale measurements of particles than are possible with sediment traps and thorium data. Thorium and sediment trap data are limited in particular by the logistics and wire time necessary to deploy and recover the required equipment.

There has been, until now, no data gathered on the size, abundance, and type of particles present throughout the entire water column across large scales in the ocean. With the development of in situ imaging systems, the spatial and temporal resolution of particle distribution, type, and size has substantially increased. The Underwater Vision Profiler 5 (UVP5) is one such instrument used to describe patterns in particles and zooplankton with high spatial resolution (Picheral et al. 2010; Forest et al. 2012; Stemmann and Boss 2012b; Biard et al. 2016; Guidi et al. 2016; Ramondenc et al. 2016). This instrument samples at finer spatial and temporal scales than more conventional methodologies such as net tows, bottle sampling, and in situ pumps, and can provide new observations of particle and zooplankton distributions and processes in the mesopelagic and bathypelagic zones. In situ imaging systems such as the UVP5 also avoid biases attributed to sediment traps related to hydrodynamics, zooplankton, and solubilization of POC (Buesseler et al. 2007). The UVP5 can be deployed across large areas allowing for snapshots of particles and zooplankton on scales difficult to access by other methods.

This study provides a full-ocean-depth ‘snapshot’ of particles and zooplankton within the water column that represent the accumulation of material present within the water column from events that happened over the past few weeks to months. The particle size distribution (PSD) revealed here are the final reflection of patterns in aggregation and fragmentation of particles (Burd and Jackson 2009). The first objective of this study is to qualitatively describe the size structure, abundance, and volume of particles through the water column across a large, diverse seascape in order to illuminate patterns in zooplankton communities synonymously with particles. The second objective is to enumerate broadscale features that can lead to mechanistic insight into vertical carbon

pumping within the ocean. This study utilizes data collected via the UVP5 in conjunction with readily-available satellite imagery to describe productivity, particle, and zooplankton patterns across a large swath of the Pacific Ocean. By looking at the patterns in productivity that coincide with the time of the collection of these data, I describe the time that it takes for particles to be injected into sub-surface layers following a phytoplankton peak, and role that zooplankton communities may play. Broad-scale collection of information about particle dynamics across diverse regions, such as this study provides, enhances our understanding of the underlying processes contributing to this important carbon export pathway.

Methods

Study Area and Sampling Strategy

The dataset herein was gathered during the CLIVAR repeat hydrography cruise P16N in 2015 (Figure 2). These data cover a large study area, spanning from 16°S to 56°N along the 150°W line of longitude sampled from April 10 to June 27, 2015. There are extremely diverse ecoregions within this span, including the Equatorial Pacific, North Pacific Gyre, and the sub-polar Gulf of Alaska. These diverse biogeographic regions have unique productivity and plankton communities which can impact particle flux. Highly-productive open ocean regions, such as the Equatorial Pacific, have the potential to contribute to carbon sequestration at a larger scale than subtropical regions, but this potential is more vulnerable to shifts in vertical mixing than corresponding changes at high latitudes (Antia et al. 2001). The oligotrophic North Pacific has low productivity due to low nutrient availability, and is therefore unlikely to be a region with high particle export. The transition zone is a highly variable area that spans the area between the northern extent of the North Pacific gyre and the southern boundary of the sub-Arctic gyre; here, we consider the bounds to be 35°N to 42°N, where the surface temperature during the sampling period was 15°C, and notably different than temperatures to the South and North. Both the transition zone and sub-Arctic Pacific are broadly described as high-nutrient low-chlorophyll (HNLC) regions. Recent evidence indicates that the North Pacific, although considered to have low seasonality and low production, could be highly productive in terms of carbon despite lacking a significant seasonal chlorophyll peak (Westberry et al. 2016). Data from long-term oceanographic station P indicate El Niño events increase particle flux (Wong et al. 1999) but the strength and transfer efficiency of the biological pump in this region remains elusive.

CTD casts to full ocean depth were performed at a distance of 0.5° latitude separation, with the exception 2°S to 2°N where tighter sampling occurred. The UVP5 was incorporated onto the CTD-rosette package and programmed to start and end acquisition based upon the instrument's internal pressure sensor. This resulted in 170 full-depth profiles parsed into 10-meter bin resolution, except where battery faults occurred, across the transect.

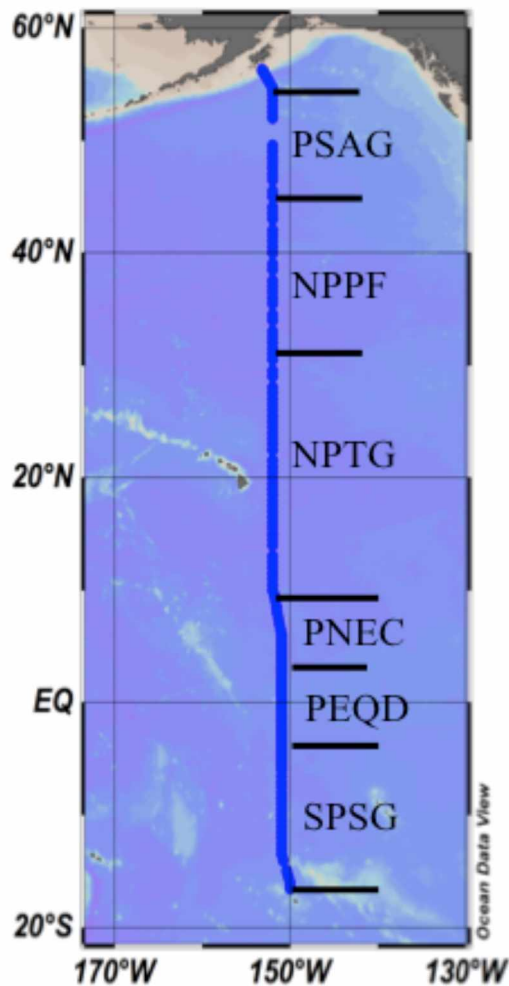


Figure 2. Station Map of P16N CLIVAR repeat hydrography cruise. Stations sampled with the UVP during the 2015 P16N CLIVAR repeat hydrography cruise. Black lines indicate the boundaries of biogeographic regions as described by Longhurst (2007): Pacific Sub-Arctic Gyre (PSAG), North Pacific Polar Front (NPPF), North Pacific Tropical Gyre (NPTG), North Pacific Equatorial Countercurrent (PNEC), Pacific Equatorial Divergence (PEQD), and South Pacific Subtropical Gyre (SPSG).

Data Collection and Processing

The Underwater Vision Profiler 5 (UVP5) is an in-situ autonomous underwater imaging instrument that collects particle size distribution data for particles 0.06 mm to 2.7 mm in diameter. The technical specifications and initial processing protocols for the UVP5 are described in Picheral et al (2010). The UVP5 used in the present study, serial number 009, was developed to withstand full ocean depth-pressure (6000m) and to be mounted on various CTD rosette frames. When deployed in mixed-processing mode the UVP5 measures and records the size and greyscale level of all objects >100 μm . Vignettes (extracted individual images) of all objects >500 μm in size are stored on internal memory for further analysis. Images were recorded at a frequency of 6 Hz.

The light from the UVP flash is known to distort the edges of imaged particles and make them appear larger, particularly for smaller objects; this bias was accounted for during the conversion from pixels to mm^2 using the power function: $\mathbf{A_m=0.0032*A_p^{1.36}}$ where $\mathbf{A_m}$ is the area in mm^2 and $\mathbf{A_p}$ is the area of the photographed particle in pixels. The constants 0.0032 and 1.36 were found through tandem deployment of this specific UVP5 with a previously calibrated UVP5 performed by immersion in a tank with known sized particles (see Picheral et al. 2010). Each UVP5 has a slightly different volume per image, the volume determined for our unit was 0.94L. These calibration factors have since been re-calculated, and will be updated before archiving of the final data. Thus, the results presented here show slightly lower numerical abundances than will be shown with final results. Equivalent spherical diameter (ESD) was calculated using the area in mm^2 of the 2-dimensional shapes captured in the image:

$$ESD = 2\sqrt{A_m/\pi}$$

Volume was calculated from ESD assuming spherical particles:

$$Volume (mm^3) = \pi ESD^3/6$$

Data from the UVP were processed and downloaded utilizing Zooprocess, a macro plugin software for the Java-based Image-J image-processing program. Only downcast data were used for both image sorting and particle volume analysis. A custom MATLAB script calculated the mean size of particle present in 10 meter depth intervals for each station using raw data produced by the instrument (Turner 2015 see Appendix). An update to the original script included the calculation of total volume of particles within each 10 meter bin for particles larger than 161 μm . Anomalous values of volume were excluded from plotting if they were 100 times larger than the volume present in either the bin above or below. These values represented rare large particles, often jellyfish, that are not representative of large scale patterns.

Image Sorting

Image sorting was accomplished using newly-developed machine-learning software EcoTaxa (Picheral et al. 2017). This tool utilized a validated training set of images to generate predicted image identities from the unsorted P16N CLIVAR dataset. After the initial prediction process was completed, images were manually validated. The manually-validated images were then be used to re-predict image identities of unvalidated images within the same dataset. The initial learning set used to predict images was provided by Marc Picheral, with an additional learning set provided by Tristan Biard from a California Current Ecosystem Long Term Ecological Research (CCE-LTER) cruise.

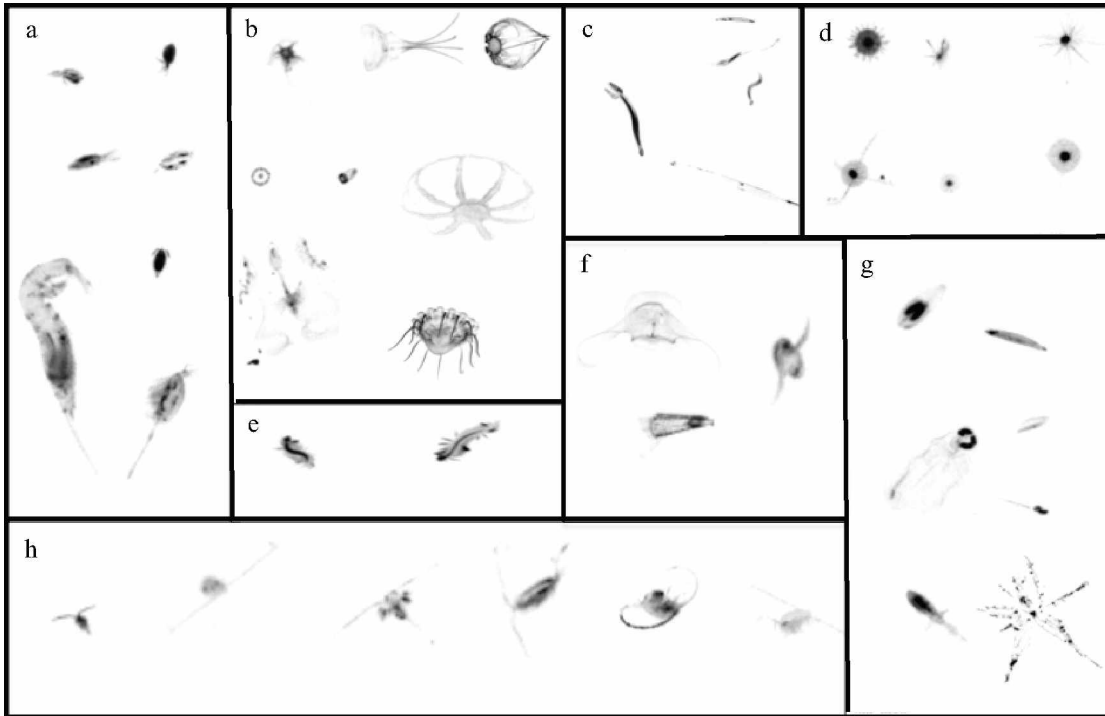


Figure 3 – Examples of zooplankton images captured by the UVP5. Images were collected during the 2015 P16N CLIVAR cruise from each sorted category: a) Crustacea (general), b) Gelatinous, c) Chaetognatha, d) Rhizaria, e) Annelida, f) Mollusca, g) Other (unknown), h) Copepoda.

The image categories chosen for this project spanned numerous zooplankton groups plus general ‘detritus’. The zooplankton categories used for this project were Annelida, Chaetognatha, Copepoda, (other) Crustacea, gelatinous, Mollusca, Rhizaria, and other (Figure 3). The gelatinous category included the following subcategories: Siphonophorae, Hydrozoa, Ctenophora, and Tunicata. The rhizaria category included the following subcategories: Acantharea, Aulacantha, Aulosphaeridae, Collodaria, colonial, solitaryblack, solitaryfuzzy, solitaryglobule, and solitarygrey. These groups were chosen based on images sorted into these categories by other EcoTaxa projects and previously published work (Picheral et al. 2010; Biard et al. 2016).

The total number of images stored by the UVP during the 152°W northern transect of the P16N cruise numbered nearly 400,000. Initially, three areas were selected for image sorting associated with interesting features in the (unsorted) particle size structure. All images were sorted from stations located within these three regions: 1.5°S to 1.5°N (equatorial), 15°N-25°N (oligotrophic gyre), and 38°N-42°N (part of the North Pacific Polar Front, NPPF – Figure 2). This approach left large latitudinal gaps in the dataset with no validated zooplankton data, so every fifth station outside of those initial regions underwent zooplankton image validation. Ultimately, over 235,000 images were sorted and validated, representing 59.7% of all images collected across the transect.

Using Data from Ecotaxa Database

After vignettes were validated, data were exported from the Ecotaxa database in station files containing information on each vignette such as validation status, image category, depth (meters), and object area (pixels - A_p). MATLAB scripts found in Appendix counted the number of each type of validated zooplankton present in 1 meter intervals at each sampled station. A MATLAB database that contained the volume of water imaged within each depth interval was provided by Marc Picheral, as this was not (at the time) part of the direct Ecotaxa export.

The abundance of particles in each size class were downloaded from the Ecotaxa particle database in detailed form, ODV format (see Appendix). Total abundance of particles was produced by summation of sizes classes at each station before plotting in Ocean Data View (ODV).

Calculation of Zooplankton Abundance

The water column was divided into vertical intervals (bins) scaled in range to maintain statistically-relevant counts of zooplankton. Zooplankton counts were considered to follow a Poisson distribution with an uncertainty of:

$$Unc = \frac{1}{\sqrt{n}}$$

where n represents the count of zooplankton. A threshold of 0.50 uncertainty was selected to determine the most appropriate vertical bin sizes for zooplankton abundance comparisons, with the goal to preserve as much vertical resolution as possible. This approach resulted in vastly different vertical bin sizes, particularly in the top 200 meters, among biogeographic regions: as high as 10 meter resolution in PSAG to as low as 100 meter resolution in NPTG. To directly compare zooplankton abundances between biogeographic regions, we selected the lower of these resolutions for the reporting of data in this study. The number of zooplankton imaged (Z_i) was divided by the volume of water imaged (V_i) to calculate zooplankton abundance (A_{zoo}) in each vertical depth bin:

$$A_{zoo} = Z_i / V_i$$

Satellite- Derived Chlorophyll-a

Surface chlorophyll-a data gathered by MODIS-Aqua and averaged across 8-days at 0.5° resolution was downloaded from the NASA Ocean Color website. This data represents an estimate of phytoplankton living in surface waters. Gaps in data were frequent, due to cloud cover. Peaks in surface chlorophyll-a were identified as values at a latitude that were at least twice the median of chlorophyll present at that latitude between April 7-June 10, 2015.

Results

Patterns in Particle Abundance, Size, Volume, and PSD

There were two locations where increased abundances of large particles were present in bathypelagic depths: around the equator and at 38°-45°N (Figure 4). Elevated abundances of particles were encountered around 53°-55°N, however, depths beyond 2000 meters were not consistently sampled in this area, so confirmation of particles through bathypelagic depths cannot be confirmed. Both microscopic particles (MiPs) 0.163-0.203 μm in size and macroscopic particles (MaPs) sized between 0.203 - 2.58 mm show higher abundances around the equator, at 38-40°N, and at 53°-55°N, the same patterns reflected in total particle abundance; both MiPs and MaPs are driving these patterns. MaPs and MiPs were abundant into bathypelagic depths around 53°-55°N, but the abundance of particles in the euphotic zone was much lower than in other regions where MiPs and MaPs were abundant to deeper depths. Mean particle size was largest in northern latitudes, particularly north of 40° (Figure 7). Larger mean sizes were most noticeable around the equator, north of 40°N and 53°-55°N.

Similar to the patterns of total particle abundance, there were two regions with elevated volumes of particles through bathypelagic depths: around the equator and 40°-43°N. A high volume of particles was also seen between 53°-56°N but, again for the reasons stated before, this pattern could only be confirmed to around 2000m (Figure 8). The penetration of large volumes of particles was strongest north of 40°N, weaker around the equator and there was no particle penetration observed within the oligotrophic gyres.

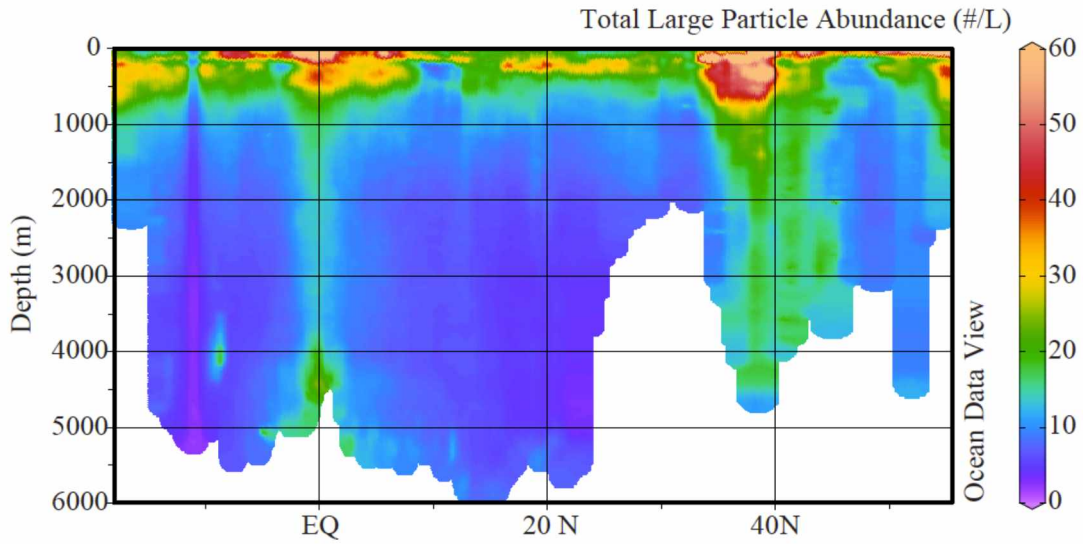


Figure 4. Total particle abundance. Total abundance of large (0.161-2.58 mm) particles (#/L) across the 2015 P16N CLIVAR cruise.

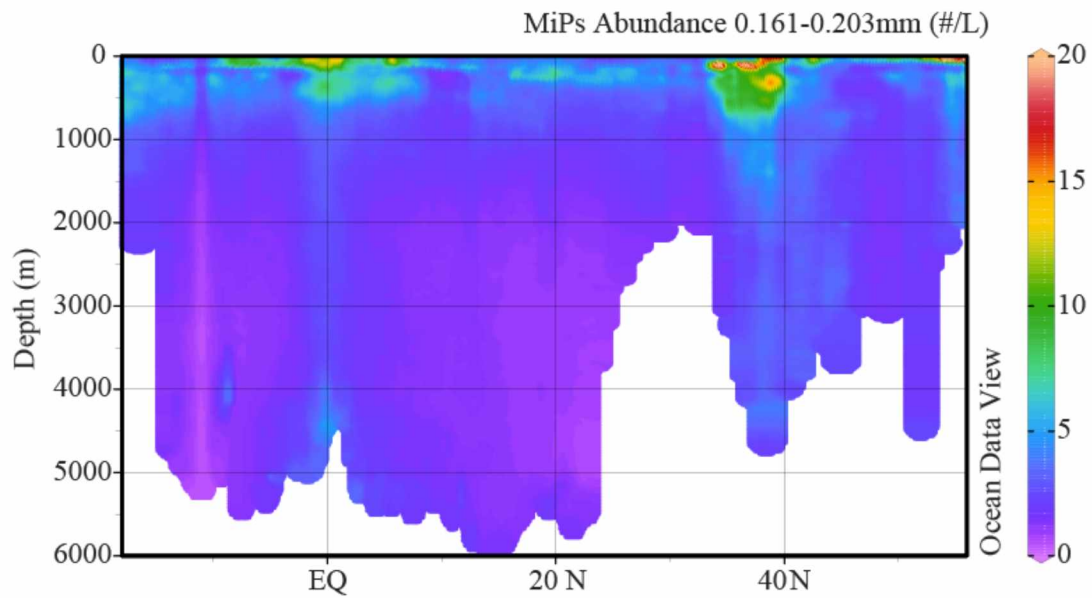


Figure 5. Microscopic particles (0.161-0.203 mm) abundance (#/L). MiPs during the 2015 P16N CLIVAR cruise.

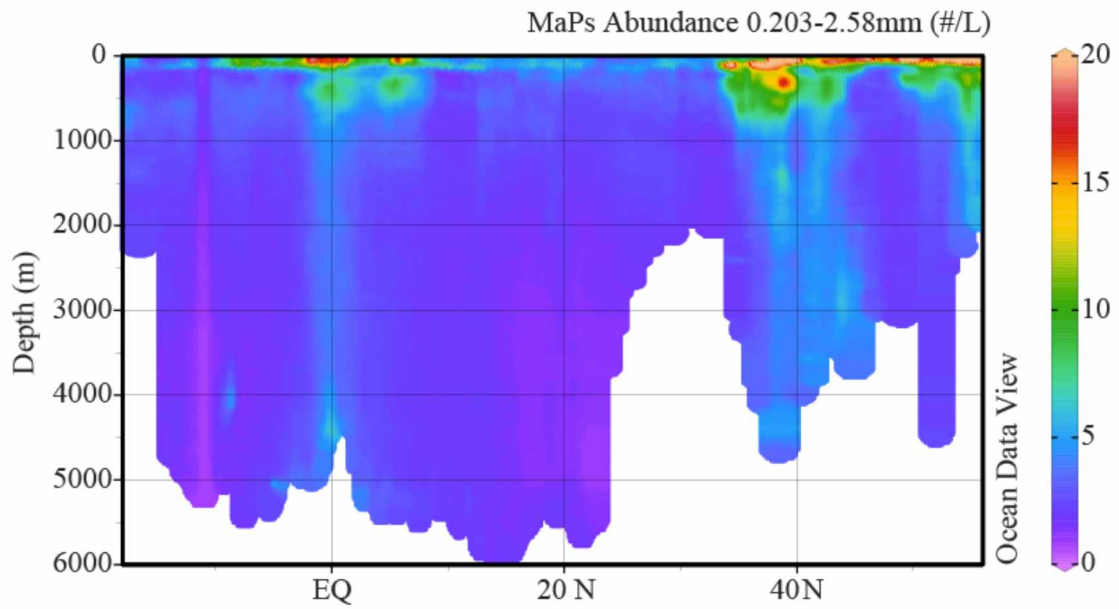


Figure 6. Macroscopic particles (0.203-2.58mm) abundance (#/L). MaPs during the 2015 P16N CLIVAR cruise.

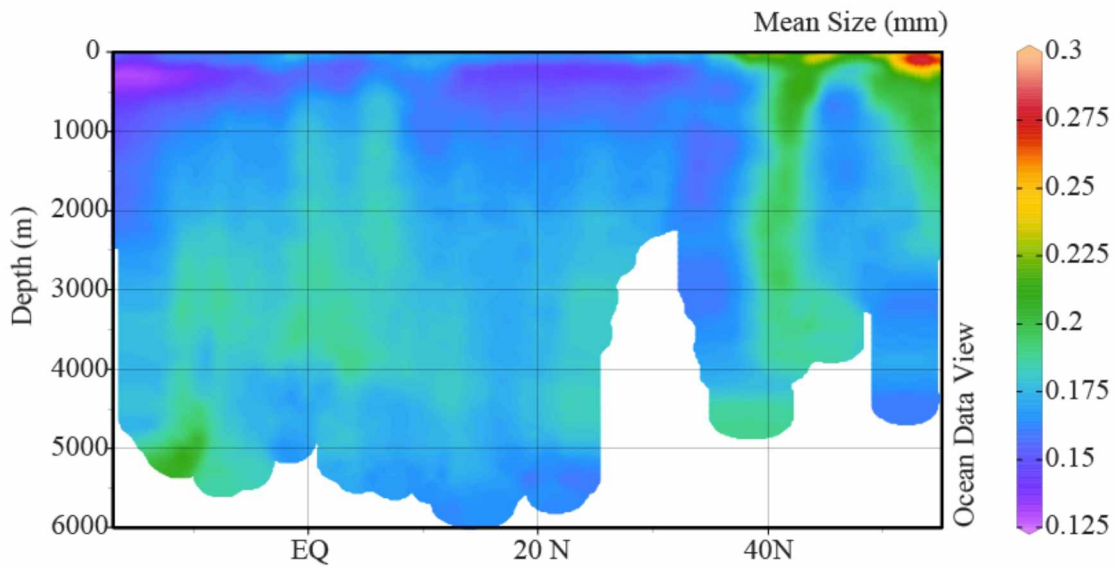


Figure 7. Mean size (mm) of particles.

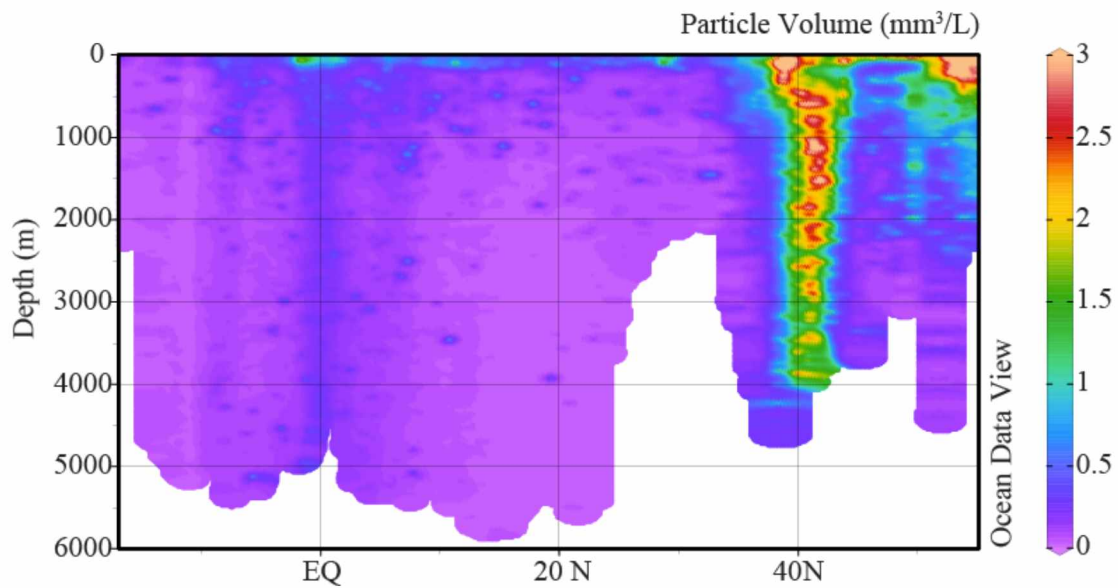


Figure 8. Particle volume ($\text{mm}^3 \text{L}^{-1}$). Total particle volume during the 2015 P16N CLIVAR cruise.

Patterns in Satellite-derived Surface Chlorophyll-a

Satellite imagery of surface chlorophyll-a showed bands of productivity throughout the sampling period (Figure 9), with higher surface chlorophyll-a along the equator and north of the oligotrophic North Pacific Gyre. The adaptive threshold of chlorophyll increases highlights four distinct times and regions where peaks in chlorophyll-a were present, indicating a phytoplankton peak: April 7-14, 2015 from 38°-40°N, May 1-8 around 42.5°N, and June 2-9, 2015 at both 45-46°N and 51°-53°N. Of particular interest is the time between when these peaks occurred and when the ship arrived and sampled the area. The peak at 38°-40°N occurred about eight weeks prior to the ship's arrival, in stark contrast to the ship's arrival about one week after the peak at 51-53°N. The ship arrived at the location of the 42.5°N peak four weeks after the peak took place and was present for the end of the peak 45-46°N, within a week after this chlorophyll max.

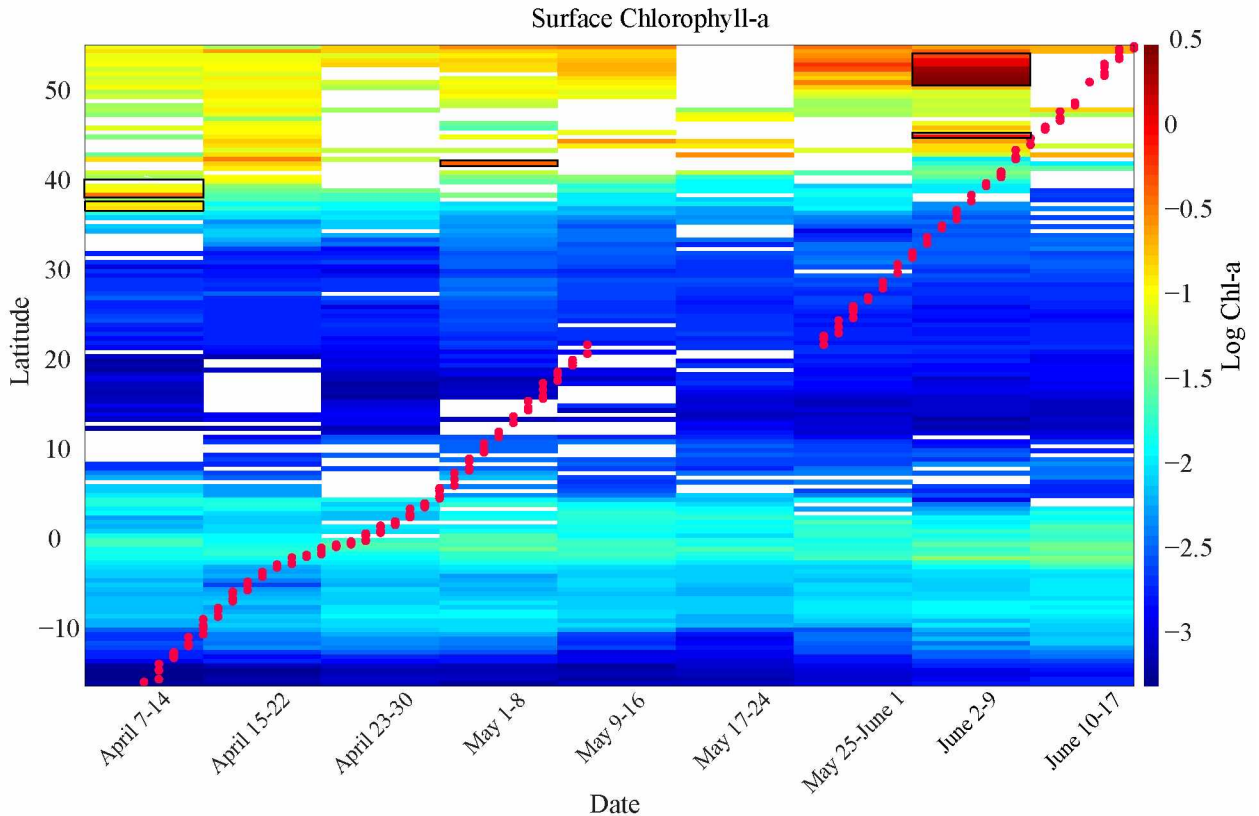


Figure 9. Surface Chlorophyll-a with cruise track. The 2015 P16N CLIVAR cruise track (red dots) superimposed across 8-day average satellite derived surface chlorophyll, with warmer colors indicating higher chlorophyll values. Chlorophyll values that were twice the median of values at the same latitude during the time which the cruise took place are highlighted with black boxes.

Patterns in Zooplankton Distribution and Abundance

Zooplankton tended to be most abundant in surface waters (<100m) and at higher latitudes across the transect. In the northernmost biogeographic region (>45°N - PSAG), high abundances of zooplankton were found in the upper mesopelagic to 500 meters (Figure 10); abundances in this region reached over 50 individuals m^{-3} . Three other regions showed noticeably high zooplankton abundances: 38-45°N (NPPF), 5°-11°N (PNEC), and 5°S to 5°N (PEQD). Significant regional variation within zooplankton abundance ($\# m^{-3}$) both in the top 100 m and 500 m was confirmed by one-way ANOVA (p-value < 0.01), with higher abundances in PSAG identified by the multicompare

function in MATLAB. These bands of high zooplankton abundance were found in conjunction with productivity patterns (see Figure 9).

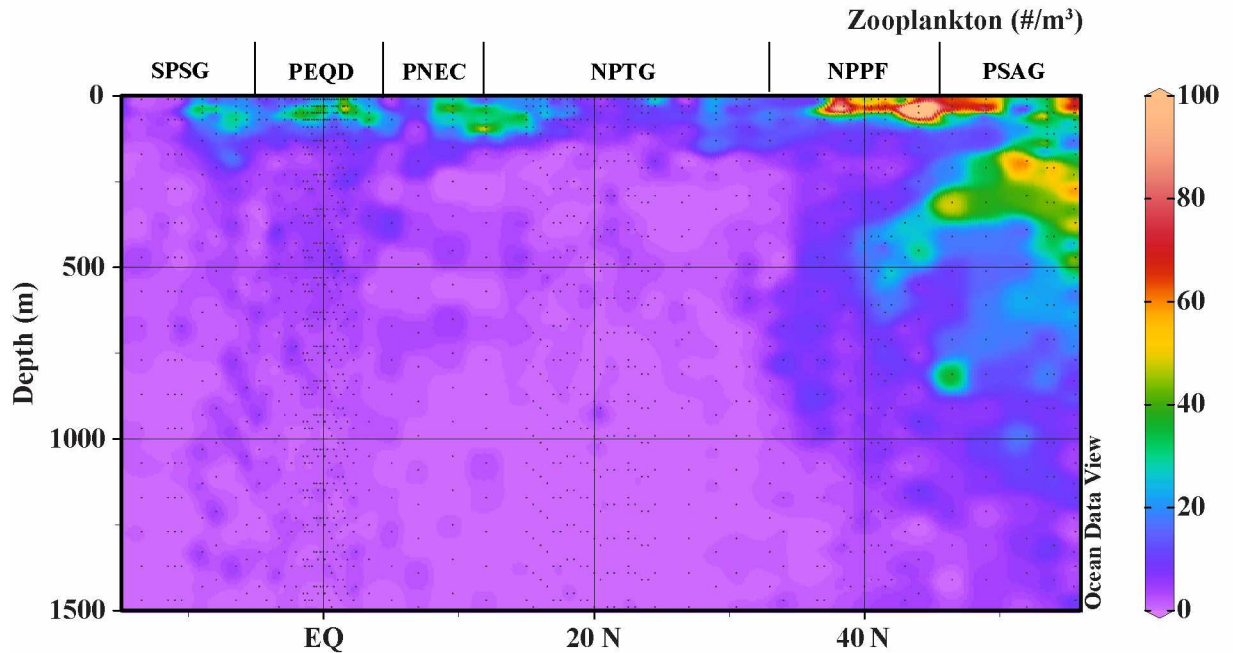


Figure 10. Zooplankton abundance ($\#/m^3$). Abundance of zooplankton across the 2015 P16N CLIVAR cruise transect of the Pacific Ocean. The biogeographic zones, in accordance with those described by Longhurst (2007), are labeled above the plot.

Community composition of zooplankton varied across biogeographic region and depth (Figure 11). Rhizaria dominated the majority of regions and depths with a noticeable exception within PSAG surface waters, where copepods and other crustaceans were the most numerically abundant. Rhizarians, copepods, and crustaceans made up over 75% of the community composition of readily identifiable zooplankton across all biogeographic regions and depth intervals. Copepods, other crustaceans, and rhizarians drove most of the variability observed in the latitudinal zooplankton distribution (Figure 12). Although dwarfed in abundance by the more numerous taxa, others group such as

annelids, chaetognaths, and gelatinous zooplankton displayed particularly patchy abundances and tend to be more common at depths below 200 meters.

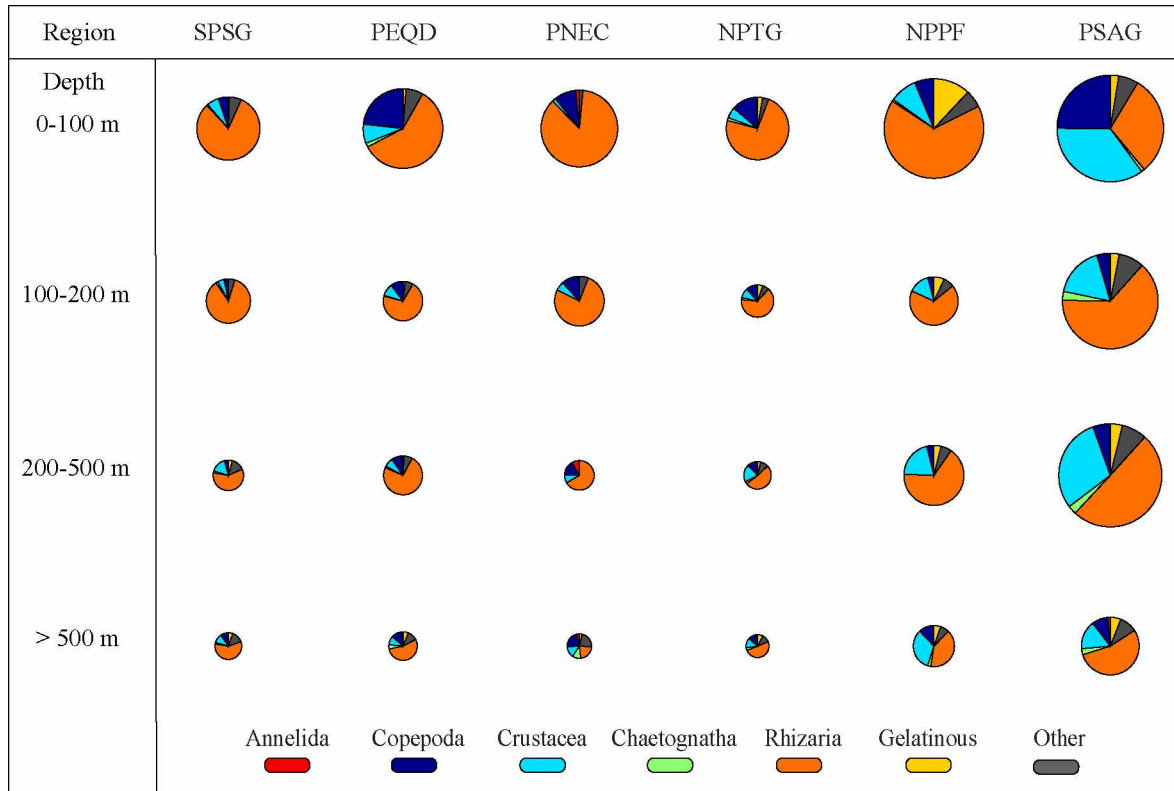


Figure 11. Zooplankton community composition. The relative contribution of zooplankton categories separated by biogeographic region and depth along the 2015 P16N CLIVAR transect. The contribution is defined as percentage of zooplankton within a depth bin, with circle size scaled to reflect average abundance within each region and depth bin. The largest average abundance (PSAG 0-100 meters) was 37.3 individuals/m³, and the smallest abundance (NPTG > 500 meters) was 1.7 individuals/m³.

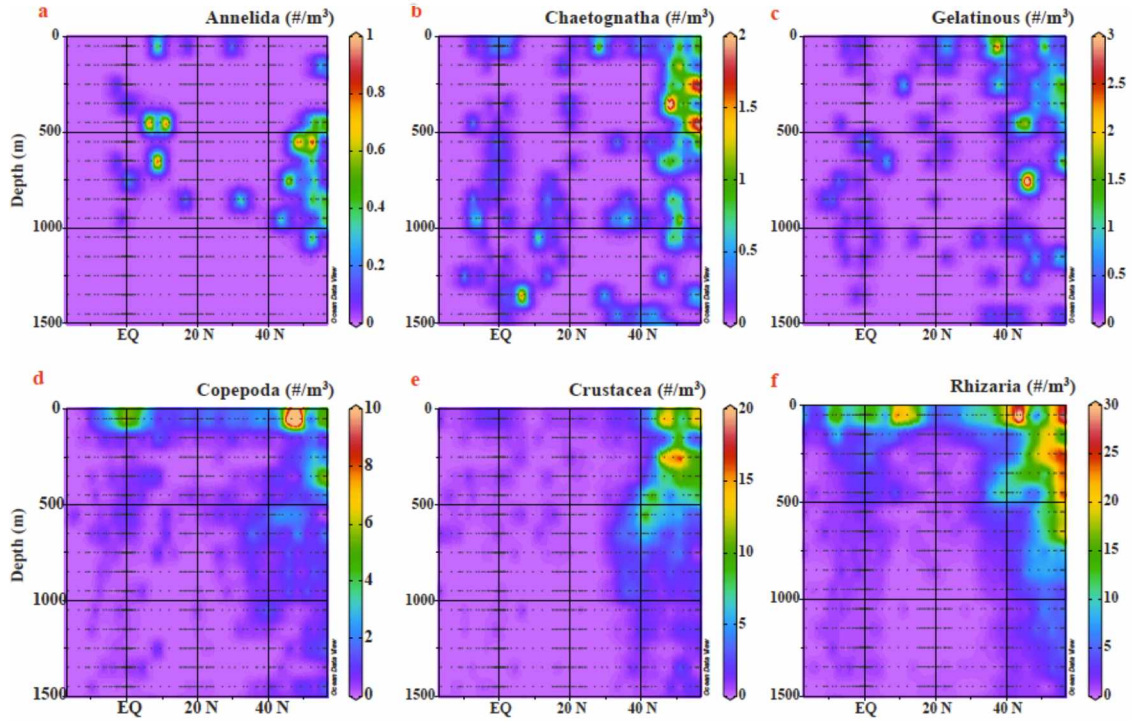


Figure 12. Abundance of zooplankton taxa. Abundance of zooplankton categories in the upper 1500m across the 2015 P16N CLIVAR transect of the Pacific Ocean. Note the different scales of abundance for each type of zooplankton: Annelida, Chaetognatha, and gelatinous abundances are enumerated using much smaller ranges than those for Copepoda, (other) Crustacea, and Rhizaria.

Discussion

The timing and large area covered by these data offer a unique snapshot of a large swath of the Pacific Ocean during an important time of year both for production, and carbon burial. By examining patterns in particles, productivity, and zooplankton, I aimed to determine whether large spatial patterns are present using optical and remote sensing methods. The dataset introduced here encompasses biologically and geographically diverse areas of the ocean and, to my knowledge, offers the first trans-Pacific, full-ocean-depth description of particle size and abundance.

Patterns in Particles Across the Pacific

Two regions contain large particles in bathypelagic waters indicating increased biological pump efficiency: beneath the equator (PEQD) and the transition zone (NPPF). The sub-Arctic Pacific (PSAG) appears to be developing a similar pattern, but particles are only present into the mesopelagic, which could be a result of either timing or an indication of strong mid-water column attenuation. This distinction among regions during the spring peak offers a unique perspective into time scales between phytoplankton peaks and the penetration of particles.

By examining a subset of the overall transect and focusing on the transition zone (NPPF) of the Pacific Ocean, this dataset captures four distinct time scales from satellite-chlorophyll peaks to when the ship arrived in the area to sample: 1) 7-8 weeks, when particles have reached deep waters all the way to the ocean floor in high numbers, but a high volume of particles was not present, 2) 4 weeks, when both abundance and volume of particles to the ocean floor were noticeably higher, 3) 1 week, when both abundance and volume of particles were high to nearly 1500 meters, but both dropped off rapidly with

increasing depth, and 4) no lag time, when the ship was sampling during the phytoplankton peak and neither abundance or volume were elevated. These observed patterns suggest that large particulate matter, created in the euphotic zone, sinks through the mesopelagic zone within a week. Within four weeks after a peak, material has made it to the seafloor. By 6-8 weeks after a phytoplankton peak the majority of material has been remineralized or disaggregated. These observations are consistent with the lower limit of estimated sinking speed, 175 meters day⁻¹ at Station P (Wong et al. 1999). In contrast, in the North Atlantic, the sinking speed of large particles has been estimated at 75 meters day⁻¹ (Briggs et al. 2011), suggesting there could be major differences in sinking speed of particles in different ocean basins. Briggs et al. (2011) interpreted glider-mounted optics to estimate aggregate sinking speeds, while Wong et al. (1999) calculated sinking rates from sediment traps. These methodological differences could be the cause for differing sinking rate estimates. These differences may also arise due to the type of aggregates that are sinking, or the zooplankton communities present within each region (Taucher et al. 2018). How quickly material sinks through the water column can be both directly and indirectly affected by zooplankton, so patterns in zooplankton abundance and composition need to be considered to help understand why some regions have particles in bathypelagic waters, while others do not.

Patterns in Zooplankton Across the Pacific

This dataset offers a unique opportunity to look at pelagic deep ocean zooplankton in addition to the typically-sampled depths near the euphotic zone. Zooplankton across this transect of the Pacific are mainly concentrated within and just below the euphotic zone, which is an expected pattern since zooplankton rely on

production from surface layers for food. The counts of zooplankton in bathypelagic depths are low, which does not allow for statistically relevant descriptions of abundance or community composition between biogeographic regions, but instead are discussed as a single, deep region. Gelatinous zooplankton, chaetognaths, and annelids all appear to have patchy abundances in these deep waters, though this apparent ‘patchiness’ could be a direct result of the low counts. The UVP may sample too small a volume to describe deep, dilute zooplankton populations, especially at the higher speeds a CTD rosette typically travels in deep water (~60 meters/minute), but the paucity of available data on bathypelagic zooplankton populations still leaves something to be gained from the information gathered. With further analysis of this dataset, and the sorting images from more stations, it may be possible to gain a better picture of the depths at which taxa are most commonly found, and particularly beyond the depths most commonly sampled with net tows.

An important pattern discovered within the zooplankton was the large numerical contribution of rhizarians to the zooplankton community across all depths and nearly all biogeographic regions. This is a surprising finding since crustaceans, and usually copepods, are thought to dominate zooplankton communities. This finding merits further scrutiny, so we compared UVP data with net tow abundances from occasion when both were deployed at the same station.

The data available for such comparison between UVP zooplankton and net-gathered zooplankton data come from the Spring 2018 Northern Gulf of Alaska Long Term Ecological Research (NGA-LTER) cruise. The station selected for comparison was an offshore station, GAK15, expecting its patterns will be most similar to the open ocean

stations of P16N. The UVP was mounted on a similarly sized CTD rosette on P16N and NGA-LTER. Multinets with 505 μ m nets were used to collect large zooplankton and partition the water column. Here, a comparison between the two zooplankton collection techniques is made for the top 100 meters of the water column (Table 1, K. Coyle and R. Hopcroft, unpublished). This comparison is primarily aimed to examine possible biases of the UVP-measured community composition data towards less motile zooplankton such as Rhizaria. Rhizaria have limited mobility and are likely unable to avoid sampling; in contrast, copepods have documented sampling avoidance associated with pressure waves generated by towing nets through the water (Fleminger and Clutter 1965). The pressure wave generated by a CTD rosette, loaded with instrumentation and bottles could very well generate a similar, if not larger pressure wave, thereby increasing the avoidance by motile zooplankton. A previous study in the Arctic indicated the UVP, while mounted on a rosette, reliably captured the abundance of copepods larger than 1mm ESD (Forest et al. 2012). Towed nets reliably sample copepods larger than 2.5 times the mesh size (Hopcroft et al. 2001), so a comparison between a 0.5 mm mesh should yield similar abundances. This comparison suggests copepods abundances are estimated to be 18 times lower with the UVP than with a net tow, while total zooplankton abundances are two times higher for UVP samples than the net tow (Table 1).

Net tows are likely to undersample Rhizaria, as they are easily destroyed by nets, and not well recognized while sorting through plankton samples (Stoecker et al. 1996); this could account for the large discrepancy in total zooplankton abundance. Nonetheless, the huge discrepancy in copepod abundance between the UVP and nets is surprising; Forest et al (2012) may not have found a similar discrepancy due to how the CTD was

loaded and deployed (and thus the generation of pressure waves). Although this single comparison is not conclusive, these data indicate there is a clear discrepancy between net tow and UVP zooplankton data in the sub-Arctic Pacific that needs to be more fully explored. It appears that while the UVP is biased against copepods, nets are even more severely biased against Rhizaria. If we assume the UVP is systematically undersampling copepods and crustaceans and apply a ‘correction factor’ of 18 to UVP copepod and crustacean abundances across the transect, rhizaria no longer dominate the community composition across regions south of PSAG.

Table 1. Comparison of zooplankton abundances from two sampling techniques: UVP and 0.5mm mesh Multinet vertical tow.

Sampling Device	Depth	Zooplankton Abundance (#/m ³)	Copepod Abundance (#/m ³)	Rhizaria Abundance (#/m ³)
UVP	0-100 meters*	468	10**	452
0.5mm Multinet	0-100 meters	201	184	N/R***

* UVP data are reported in 5-meter depth bins, so data were integrated over the top 100 meters for this table

** All crustaceans are reported in aggregate

*** Presence was not reported (N/R)

Whether Rhizaria are more abundant than copepods or not, these large protists appear to be mostly ignored in zooplankton assessment throughout the Pacific Ocean (Stoecker et al. 1996; Biard et al. 2016). Little is known about these large protists; attempts to estimate the role of Rhizaria in the carbon (Stukel et al. 2018) and silica cycles (Biard et al. 2018) reveal large gaps in our ability to estimate the biomass and metabolic requirements of these plankton. Other optical plankton instruments have also suggested the abundance of Rhizaria may be severely underestimated by several orders of

magnitude (Dennett et al. 2002). Larger abundances of protists, particularly foraminifera and acantharea, have been associated with El Nino patterns in the equatorial region (Stoecker et al. 1996); the strong El Nino in the Pacific through 2015 very likely contributed to the high abundances of Rhizaria noted here.

If large Rhizaria follow similar grazing habits as their smaller relatives, then they are likely grazing down a large portion of the phytoplankton community across much of the open ocean (Calbet and Landry 2004). Rhizaria have been identified as a culprit for increased particle attenuation due to their ability to capture sinking particles, which are some rhizarian's primary food source (Stukel et al. 2018). The generational turnover of some phaeodarians (type of rhizaria) has been estimated as ~5 days, while deeper dwelling species are slower growing and have a longer turnover time, ~10 days (Stukel et al. 2018). These turnover times and feeding habits can explain why abundances of Rhizaria are greater around 200 meters compared to euphotic depths more than a week after a peak in PSAG. What little we do know about Rhizaria life histories, combined with their large abundances revealed in this study, highlight the importance of analyzing rhizarians alongside particles counts. This relationship, as well as total zooplankton abundance relative to particles, is discussed below.

Connecting Particles and Zooplankton

Two key features connect the regions with high abundances of particles in bathypelagic waters (PEQD and NPPF); the first feature is a high abundance of zooplankton in surface waters. Within these clusters of zooplankton both the size and abundance of particles decrease, while the volume and size of particles below the clusters increases. This pattern suggests zooplankton communities initially attenuate the flux of

material (Taucher et al. 2018), then repackage material into larger parcels such as fecal pellets. Large abundances of particles in deep waters are due to repackaging by zooplankton and passive aggregation unrelated to zooplankton (Stemmann et al. 2004b; Burd and Jackson 2009). The relative contribution of each process is not yet ascertainable.

The second feature shared between PEQD and NPPF is their designation as high-nutrient, low-chlorophyll (HNLC) regions (Minas et al. 1986). This connection is especially important when considering the link between zooplankton and particle transport in these areas. Zooplankton primarily contribute to particle transport in HNLC regions through fecal pellet production both in the euphotic at low latitudes (Kiko et al. 2017) and in the mesopelagic at high latitudes (Le Borgne and Rodier 1997). The increase in size and abundance of particles beneath zooplankton clusters in PEQD and NPPF could very likely be a result of fecal pellet production. If this is an HNLC shared pattern, why is this pattern missing in the other HNLC region, PSAG? This difference might be explained by the deep-dwelling rhizaria populations in PSAG intercepting sinking particulates in their extra-capsular cytoplasm and attenuating flux (Boltovskoy 1999). Protozoan ingestion instead of zooplankton grazing has been postulated as the controlling factor preventing large phytoplankton peaks in HNLC regions (Capriulo et al. 1991; Landry et al. 1993). It remains unknown whether this attenuation pattern is persistent or if it is merely an artifact of sampling closer in time to a phytoplankton peak. Deeper analysis of these data in future studies could shed some light on the connections identified here.

Conclusions

This study reveals HNLC regions to be of particular importance for consideration as areas of increased carbon sequestration. Overall large-scale features in particles follow overlying patterns of productivity, however, our results indicate that timing also plays a role in sub-regional features as it relates to depth. Large abundances of zooplankton are present in the areas where particles penetrate deepest into the ocean though their role in the magnitude of flux remains elusive; high abundances of large *Rhizaria* may attenuate flux.

These data offer an important snapshot of where particles sink into the deep sea, carrying carbon for long-term storage away from the atmosphere. A time-series of a few stations in one or more of these HNLC regions would prove extremely valuable to determine if these patterns result from seasonal productivity, or are sustained. Studies have already begun to model the aggregation and disaggregation patterns of particles, using the particle size-structure data presented here (Cram et al. 2018). Modeling has helped constrain our understanding of where particles are disaggregating and aggregating, while this study is chipping away at the potential answers to 'how'. High zooplankton abundances have now been shown to be associated with large particle penetration into bathypelagic waters. To examine the mechanistic relationship, more detailed productivity and zooplankton data should be collected in tandem with particle analysis, such as is occurring during the EXPORTS campaign. We have yet to introduce size-structured zooplankton, as is present in the current data, into biogeochemical cycling models that already include phytoplankton (Ward et al. 2012); this could further our understanding of how zooplankton influence global scale patterns of both carbon and

nutrients. This study has highlighted three distinct regions to focus upon the biological pump within the Pacific Ocean, allowing future time and energy to be applied to the most promising regions of the oceanic Pacific for carbon burial.

References

- Allredge, A. 2005. The contribution of discarded appendicularian houses to the flux of particulate organic carbon from oceanic surface waters, p. 309–326. *In* G. Gorsky, M.J. Youngbluth, and D. Deibel [eds.], *Response of Marine Ecosystems to Global Change: Ecological Impact of Appendicularia*.
- Antia, N., R. Peinert, D. Hebbeln, U. Bathmann, U. Fehner, and B. Zeitzschel. 2001. Basin-wide particulate carbon flux in the Atlantic Ocean: regional export patterns and potential for atmospheric CO₂ sequestration. *Global Biogeochem. Cycles* **15**: 845–862. doi:10.1029/2000gb001376
- Biard, T., J. W. Krause, M. R. Stukel, and M. D. Ohman. 2018. The significance of giant Phaeodarians (Rhizaria) to biogenic silica export in the California current ecosystem. *Global Biogeochem. Cycles* **32**: 987–1004. doi:10.1029/2018GB005877
- Biard, T., L. Stemann, M. Picheral, and others. 2016. In situ imaging reveals the biomass of giant protists in the global ocean. *Nature* **532**: 1–16. doi:10.1038/nature17652
- von Bodungen, B., A. Anita, E. Bauderfiend, and others. 1995. Pelagic processes and vertical flux of particles : an overview of a long-term comparative study in the Norwegian Sea and Greenland Sea. *Geol Rundsch* **84**: 11–27.
- Boltovskoy, D. 1999. *Radiolaria Polycystina*, D. Boltovskoy [ed.]. Backhuys Publishers, Leiden.
- Le Borgne, R., and M. Rodier. 1997. Net zooplankton and the biological pump: a comparison between the oligotrophic and mesotrophic equatorial Pacific. *Deep. Res. Part II Top. Stud. Oceanogr.* **44**: 2003–2023. doi:10.1016/S0967-0645(97)00034-9
- Boyd, P. W., and T. W. Trull. 2007. Understanding the export of biogenic particles in oceanic waters: is there consensus? *Prog. Oceanogr.* **72**: 276–312. doi:10.1016/j.pocean.2006.10.007
- Briggs, N., M. J. Perry, I. Cetinić, C. Lee, E. D'Asaro, A. M. Gray, and E. Rehm. 2011. High-resolution observations of aggregate flux during a sub-polar North Atlantic spring bloom. *Deep. Res. Part I Oceanogr. Res. Pap.* **58**: 1031–1039. doi:10.1016/j.dsr.2011.07.007
- Buesseler, K. O., A. N. Antia, M. Chen, and others. 2007. An assessment of the use of sediment traps for estimating upper ocean particle fluxes. *J. Mar. Res.* **65**: 345–416. doi:10.1357/002224007781567621

- Buesseler, K. O., and P. W. Boyd. 2009. Shedding light on processes that control particle export and flux attenuation in the twilight zone of the open ocean. *Limnol. Oceanogr.* **54**: 1210–1232.
- Burd, A. B., and G. A. Jackson. 2009. Particle aggregation. *Ann. Rev. Mar. Sci.* **1**: 65–90. doi:10.1146/annurev.marine.010908.163904
- Calbet, A., and M. R. Landry. 2004. Phytoplankton growth, microzooplankton grazing, and carbon cycling in marine systems. *Limnol. Oceanogr.* **49**: 51–57. doi:10.4319/lo.2004.49.1.0051
- Capriulo, G. M., E. M. Sherr, and B. F. Sherr. 1991. Trophic behavior and related community feeding activities of heterotrophic marine protists, p. 219–265. *In* P.C. Reid, C.M. Turley, and P.H. Burkhill [eds.], *Protozoa and their Role in Marine Processes*. Springer.
- Cram, J. A., T. Weber, S. W. Leung, J. Liang, and C. Deutsch. 2018. Global Biogeochemical Cycles The Role of Particle Size , Ballast , Temperature , and Oxygen in the Sinking Flux to the Deep Sea. 858–876. doi:10.1029/2017GB005710
- Dennett, M. R., D. A. Caron, A. F. Michaels, S. M. Gallager, and C. S. Davis. 2002. Video plankton recorder reveals high abundances of colonial Radiolaria in surface waters of the central North Pacific. *J. Plankton Res.* **24**: 797–805.
- Dilling, L., and A. L. Alldredge. 2000. Fragmentation of marine snow by swimming macrozooplankton: A new process impacting carbon cycling in the sea. *Deep. Res. Part I Oceanogr. Res. Pap.* **47**: 1227–1245. doi:10.1016/S0967-0637(99)00105-3
- Fleminger, A., and R. I. Clutter. 1965. Avoidance of towed nets by zooplankton. *Limnol. Oceanogr.* **10**: 96–104.
- Forest, a., L. Stemmann, M. Picheral, L. Burdorf, D. Robert, L. Fortier, and M. Babin. 2012. Size distribution of particles and zooplankton across the shelf-basin system in southeast Beaufort Sea: Combined results from an Underwater Vision Profiler and vertical net tows. *Biogeosciences* **9**: 1301–1320. doi:10.5194/bg-9-1301-2012
- Gehlen, M., L. Bopp, N. Emprin, O. Aumont, C. Heinze, O. Ragueneau, D. Mer, and P. Copernic. 2006. Reconciling surface ocean productivity, export fluxes and sediment composition in a global biogeochemical ocean model. *Biogeosciences* **3**: 521–537.
- Giesecke, R., H. E. González, and U. Bathmann. 2010. The role of the chaetognath *Sagitta gazellae* in the vertical carbon flux of the Southern Ocean. *Polar Biol.* **33**: 293–304. doi:10.1007/s00300-009-0704-4

- Guidi, L., S. Chaffron, L. Bittner, and others. 2016. Plankton networks driving carbon export in the oligotrophic ocean. *Nature* 465–470. doi:10.1038/nature16942
- Guidi, L., G. A. Jackson, L. Stemann, J. Carlos, M. Picheral, and G. Gorsky. 2008. Relationship between particle size distribution and flux in the mesopelagic zone. *Deep. Res. Part I* 55: 1364–1374. doi:10.1016/j.dsr.2008.05.014
- Henson, S. A., R. Sanders, and E. Madsen. 2012. Global patterns in efficiency of particulate organic carbon export and transfer to the deep ocean. *Global Biogeochem. Cycles* 26: 1–14. doi:10.1029/2011GB004099
- Honjo, S., B. J. Hay, S. J. Manganini, and others. 1987. Seasonal cyclicity of lithogenic particle fluxes at a southern Black Sea sediment trap station. *SCOPE/UNEP Sonderband H.* 62 19–39.
- Honjo, S., S. J. Manganini, R. A. Krishfield, and R. Francois. 2008. Particulate organic carbon fluxes to the ocean interior and factors controlling the biological pump: A synthesis of global sediment trap programs since 1983. *Prog. Oceanogr.* 76: 217–285. doi:10.1016/j.pcean.2007.11.003
- Hopcroft, R. R., J. Roff, and F. P. Chavez. 2001. Size paradigms in copepod communities: a re-examination. *Hydrobiologia* 453/454: 133–141.
- Jackson, G. A., R. Maffione, D. K. Costello, A. L. Alldredge, B. E. Logan, and H. G. Dam. 1997. Particle size spectra between 1 μ m and 1 cm at Monterey Bay determined using multiple instruments. *Deep. Res.* 44: 1739–1767.
- Kiko, R., A. Biastoch, P. Brandt, and others. 2017. Biological and physical influences on marine snowfall at the equator. *Nat. Geosci.* 10: 852–858. doi:10.1038/NGEO3042
- De La Rocha, C. L., and U. Passow. 2007. Factors influencing the sinking of POC and the efficiency of the biological carbon pump. *Deep. Res. Part II Top. Stud. Oceanogr.* 54: 639–658. doi:10.1016/j.dsr2.2007.01.004
- Lam, P. J., and O. Marchal. 2015. Insights into Particle Cycling from Thorium and Particle Data. *Ann. Rev. Mar. Sci.* 7: 159–184. doi:10.1146/annurev-marine-010814-015623
- Landry, M. R., B. C. Monger, and K. E. Selph. 1993. Time-dependency of microzooplankton grazing and phytoplankton growth in the subarctic Pacific. *Prog. Oceanogr.* 32: 205–222. doi:10.1016/0079-6611(93)90014-5
- Longhurst, A. 2007. *Ecological Geography of the Sea*, Second. Elsevier Inc.
- Maier-reimer, E., U. Mikolajewicz, and A. Winguth. 1996. Future ocean uptake of CO₂: interaction between ocean circulation and biology. *Clim. Dyn.* 12: 711–721.

- Manno, C., V. Tirelli, A. Accornero, and S. Fonda Umani. 2010. Importance of the contribution of *Limacina helicina* faecal pellets to the carbon pump in terra nova bay (Antarctica). *J. Plankton Res.* **32**: 145–152. doi:10.1093/plankt/fbp108
- Marsay, C. M., R. J. Sanders, S. A. Henson, K. Pabortsava, and E. P. Achterberg. 2014. Attenuation of sinking particulate organic carbon flux through the mesopelagic ocean. *Proc. Natl. Acad. Sci.* **112**: 1089–1094. doi:10.1073/pnas.1415311112
- Martin, J. H., G. A. Knauer, D. M. Karl, and W. W. Broenkow. 1987. VERTEX: carbon cycling in the northeast Pacific. *Deep Sea Res. Part A, Oceanogr. Res. Pap.* **34**: 267–285. doi:10.1016/0198-0149(87)90086-0
- McDonnell, A. M. P., and K. O. Buesseler. 2010. Variability in the average sinking velocity of marine particles. *Limnol. Oceanogr.* **55**: 2085–2096. doi:10.4319/lo.2010.55.5.2085
- McDonnell, A. M. P., and K. O. Buesseler. 2012. A new method for the estimation of sinking particle fluxes from measurements of the particle size distribution, average sinking velocity, and carbon content. *Limnol. Oceanogr. Methods* **10**: 329–346. doi:10.4319/lom.2012.10.329
- McDonnell, A. M. P., P. J. Lam, C. H. Lamborg, and others. 2015. The oceanographic toolbox for the collection of sinking and suspended marine particles. *Prog. Oceanogr.* doi:10.1016/j.pocean.2015.01.007
- Minas, H. J., M. Minas, and T. T. Packard. 1986. Productivity in upwelling areas deduced from hydrographic and chemical fields. *Limnol. Oceanogr.* **31**: 1182–1206.
- Picheral, M., S. Colin, and J.-O. Irisson. 2017. EcoTaxa, a tool for the taxonomic classification of images. <http://ecotaxa.obs-vlfr.fr>.
- Picheral, M., L. Guidi, L. Stemmann, D. M. Karl, G. Iddaoud, and G. Gorsky. 2010. The Underwater Vision Profiler 5: An advanced instrument for high spatial resolution studies of particle size spectra and zooplankton. *Limnol. Oceanogr. Methods* **8**: 462–473. doi:10.4319/lom.2010.8.462
- Ramondenc, S., F. Lombard, C. Santinelli, L. Stemmann, G. Gorsky, and L. Guidi. 2016. An initial carbon export assessment in the Mediterranean Sea based on drifting sediment traps and the Underwater Vision Profiler data sets. *Deep. Res. Part I* **117**: 107–119. doi:10.1016/j.dsr.2016.08.015
- Sarmiento, J. L., and N. Gruber. 2006. *Ocean Biogeochemical Dynamics*, Princeton University Press.

- Sarmiento, J. L., and C. Le Quéré. 1996. Oceanic carbon dioxide uptake in a model of century-scale global warming. *Science* (80-.). **274**: 1346–1350. doi:10.1126/science.274.5291.1346
- Sarmiento, J. L., and J. R. Toggweiler. 1984. A new model for the role of the oceans in determining atmospheric pCO₂. *Nature* **308**: 621–624. doi:10.1038/311525a0
- Savoie, N., T. W. Trull, S. H. M. Jacquet, J. Navez, and F. Dehairs. 2008. Th-based export fluxes during a natural iron fertilization experiment in the Southern Ocean (KEOPS). *Deep Sea Res. II* **55**: 841–855. doi:10.1016/j.dsr2.2007.12.036
- Siegel, D. A., K. O. Buesseler, M. J. Behrenfeld, and others. 2016. Prediction of the Export and Fate of the Global Ocean Net Primary Production: The EXPORTS Science Plan. *Front. Mar. Sci.* **3**: 22. doi:10.3389/fmars.2016.00022
- Stemmann, L., and E. Boss. 2012a. Plankton and Particle Size and Packaging: From Determining Optical Properties to Driving the Biological Pump. *Ann. Rev. Mar. Sci.* **4**: 263–290. doi:10.1146/annurev-marine-120710-100853
- Stemmann, L., and E. Boss. 2012b. Plankton and Particle Size and Packaging: From Determining Optical Properties to Driving the Biological Pump. *Ann. Rev. Mar. Sci.* **4**: 263–290. doi:10.1146/annurev-marine-120710-100853
- Stemmann, L., G. A. Jackson, and G. Gorsky. 2004a. A vertical model of particle size distributions and fluxes in the midwater column that includes biological and physical processes - Part II: Application to a three year survey in the NW Mediterranean Sea. *Deep. Res. Part I* **51**: 885–908. doi:10.1016/j.dsr.2004.03.002
- Stemmann, L., G. A. Jackson, and D. Ianson. 2004b. A vertical model of particle size distributions and fluxes in the midwater column that includes biological and physical processes — Part I: model formulation. *Deep. Res. Part I* **51**: 865–884. doi:10.1016/j.dsr.2004.03.001
- Stoecker, D. K., D. E. Gustafson, and P. G. Verity. 1996. Micro- and mesoprotozooplankton at 140° W in the equatorial Pacific: heterotrophs and mixotrophs. *Aquat. Microb. Ecol.* **10**: 273–282.
- Stukel, M. R., T. Biard, J. Krause, and M. D. Ohman. 2018. Large Phaeodaria in the twilight zone: Their role in the carbon cycle. *Limnol. Oceanogr.* 1–16. doi:10.1002/lno.10961
- Taucher, J., P. Stange, M. Algueró-muñiz, L. T. Bach, A. Nauendorf, R. Kolzenburg, J. Büdenbender, and U. Riebesell. 2018. Progress in Oceanography In situ camera observations reveal major role of zooplankton in modulating marine snow formation during an upwelling-induced plankton bloom. *Prog. Oceanogr.* **164**: 75–88. doi:10.1016/j.pocan.2018.01.004

- Toggweiler, J. R., R. Murnane, S. Carson, A. Gnanadesikan, and J. L. Sarmiento. 2003. Representation of the carbon cycle in box models and GCMs 2. Organic pump. *Global Biogeochem. Cycles* **17**. doi:10.1029/2001GB001841
- Trull, T. W., and L. Armand. 2001. Insights into Southern Ocean carbon export from the C of particles and dissolved inorganic carbon during the SOIREE iron release experiment. *Deep. Res. Part II* **48**: 2655–2680.
- Turner, J. 2015. Investigating marine particle distributions and processes using in situ imaging in the Gulf of Alaska. University of Alaska Fairbanks.
- Volk, T., and M. I. Hoffert. 1985. Ocean Carbon Pumps: Analysis of Relative Strengths and Efficiencies in Ocean-Driven Atmospheric CO₂ Changes. *Geophys. Monogr. Ser.* **32**: 99–110.
- Ward, B. A., S. Dutkiewicz, O. Jahn, and M. J. Follows. 2012. A size-structured food-web model for the global ocean. *Limnol. Oceanogr.* **57**: 1877–1891. doi:10.4319/lo.2012.57.6.1877
- Westberry, T. K., M. J. Behrenfeld, P. Schultz, J. P. Dunne, M. R. Hiscock, S. Maritorena, J. L. Sarmiento, and D. A. Siegel. 2016. Annual cycles of phytoplankton biomass in the subarctic Atlantic and Pacific Ocean. *Global Biogeochem. Cycles* **30**: 1–16. doi:10.1002/2015GB005276.
- Wong, C. S., F. A. Whitney, D. W. Crawford, K. Iseki, R. J. Matear, W. K. Johnson, J. S. Page, and D. Timothy. 1999. Seasonal and interannual variability in particle fluxes of carbon, nitrogen and silicon from time series of sediment traps at Ocean Station P, 1982-1993: Relationship to changes in subarctic primary productivity. *Deep. Res. Part II Top. Stud. Oceanogr.* **46**: 2735–2760. doi:10.1016/S0967-0645(99)00082-X

Appendix

UVP Data Download and Initial Processing Workflow

- 1) Download raw files to project folder
- 2) Open raw folder and check whether .bmp images are present in raw folder, or are within a subfolder
 - a. If subfolders are present (Usually titled '00', '01' etc), cut and paste or copy contents of subfolder to the raw folder. Without this step, zooprocess is not able to find PID/vignettes so they will not be processed
- 3) Copy down UVP filename and determine which CTD cast/event each file is associated with
 - a. UVP filename format: HDRyyyymmddhhmmss
 - i. If there is not an event/cast time that is associated with a filename (or if this is a repeated issue) confirm the UVP and associated laptop are in UTC time.
- 4) Enter UVP filename into comment section of Eventlogger on CTD deployment event in the following format: UVP:HDRyyyymmddhhmmss
- 5) Copy and paste eventlogger into notepad (or save eventlogger as text file if possible) and save file as Eventlogger.txt
- 6) Run Metadata_build.m file
 - a. When prompted asking whether you would like to use previously determined downcast, select 'YES'
 - b. Choose appropriate downcast limits for each new cast
 - i. Currently the line to indicate where downcast choices are goes to 1000 meters, but if you have deeper casts you will need to change this limit (shallower casts will be ok)
- 7) Once the new metadata file has been processed, copy built metadata file 'uvp5_header...' in 'docs' folder to 'meta' folder and replace the file already present
- 8) Process .dat and .bru in Zooprocess
 - a. Open ImageJ
 - b. From the dropdown menu, select 'Process DAT BRU and VIGNETTES'

- c. Select the following options:
 - i. Process dat and bru
 - ii. Plot Profiles
 - iii. Skip Processed Files
 - iv. Batch Process
 - d. Processing should take about 15 minutes for processing only dat and bru files for ~ 20 profiles gathered using 'Depth trigger' mode. This time could be longer for I/O mode started casts.
- 9) When ImageJ/Zooprocess is finished (first screen with dropdown menu appears) open MATLAB
- 10) Create new folder named 'analysis' in project folder
- 11) Prepare UVP_Process_'CRUISEID'.m – This file needs to be adapted for use on each cruise and is going to differ slightly depending on which UVP (sn009 or sn207) the data being processed is from
- a. Copy and paste into new .m file a previous version of UVP_Process script and change the following:
 - i. Search for old project name " uvp5_sn###_....." and replace with new project name that was created in zooprocess: 4 places to change
 - 1. Line 6 project_name
 - 2. Line 10 output_dir
 - 3. Line 27 readdir
 - 4. Line 28 metadir
 - ii. Enter the metadata filename you want to process at line 33 'meta_filename'
 - 1. The metadata filename is going to be how the project workspace will be titled (See line 382 'save.....')
 - 2. If you want to process sections of the project instead of the whole thing, you can create a different metadata file and make 'subsets' of the whole project to visualize

- a. Make sure you are aware where the output is saved, and change as you see fit to organize subsets
 - iii. Change longitude (line 142) and latitude (143) for plotting of stations (figure 1)
 - iv. Check that correct pixel size as well as 'Aa' & 'bb' are correct for camera
 - 1. Line 191 – pixmm
 - a. 0.097 (sn207)
 - b. 0.1469 (sn009)
 - 2. Line 192 – Aa
 - a. 0.0032 (sn207)
 - b. 0.0092 (sn009)
 - 3. Line 193 – bb
 - a. 1.19 (sn207)
 - b. 1.21 (sn009)
 - 4. Line 300 & 301 – adj
 - a. All 1's for sn207 as adjustment is not needed
 - b. Uncomment line 300 and comment out 301 for sn009 adjustment factors (maybe?? We should check on this with new calibrations)

12) Making these corrections, leaving all sections beyond line 391 commented out will allow for the following variables to be calculated

- a. CSD - Size distribution not normalized
- b. CSDn - normalized size distribution
- c. Ms_proj - Mean size (mm)
- d. Gs_proj - mean greyscale
- e. C_total_proj - total abundance of particles per Liter

13) If you want to visualize data more steps are needed:

- a. Make sure 'cm.m' is copied from a previous project into the 'analysis' folder
 - i. This is a colormap that helps emphasize low values

- b. Change ranges both in depth and latitude/longitude for figures in order to properly plot data

Basic Steps to Import Projects into Ecotaxa Database

1) Upload Whole Project onto Ecotaxa FTP Server UNZIPPED

FTP Log-in:

host : plankton.obs-vlfr.fr

username: ftp_plankton

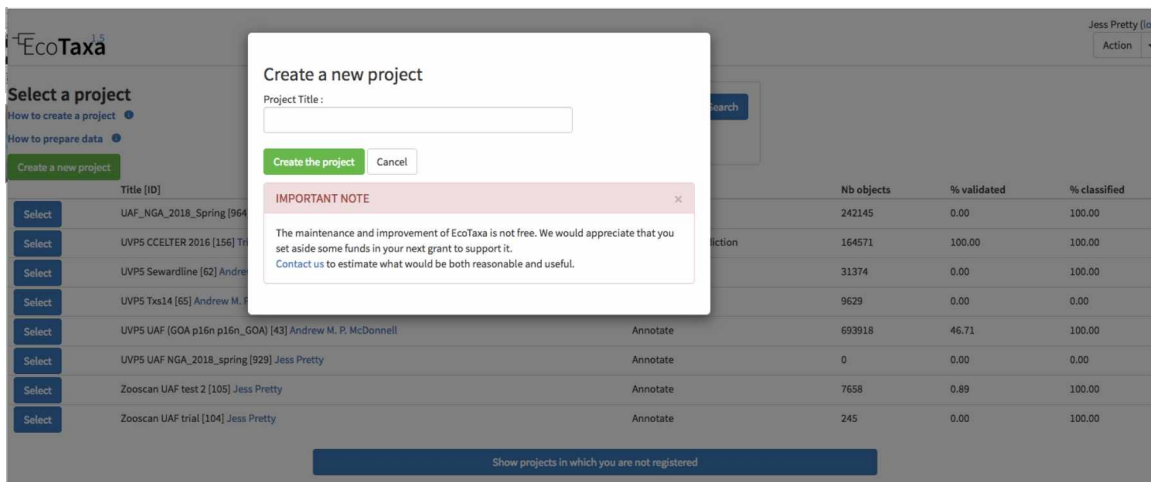
password: Pl@nkt0n4Ecotaxa

Folder to upload to: UVP5_UAF_data

2) Log in to Ecotaxa and select “Create New Project”

3) Upload files from FTP site to Ecotaxa:

For Image Database, only upload ‘Work’ Folder when prompted to import data as shown below.



The screenshot shows the EcoTaxa web interface. A modal dialog box titled "Create a new project" is open, featuring a "Project Title:" input field, a "Create the project" button, and a "Cancel" button. Below the dialog, a pink "IMPORTANT NOTE" banner reads: "The maintenance and improvement of EcoTaxa is not free. We would appreciate that you set aside some funds in your next grant to support it. Contact us to estimate what would be both reasonable and useful." The background shows a table of projects with columns for "Title [ID]", "Nb objects", "% validated", and "% classified".

Title [ID]	Nb objects	% validated	% classified
UAF_NGA_2018_Spring [964]	242145	0.00	100.00
UVP5 CCELTAR 2016 [156] Tr	164571	100.00	100.00
UVP5 Sewardline [62] Andre	31374	0.00	100.00
UVP5 Txs14 [65] Andrew M. I	9629	0.00	0.00
UVP5 UAF (GOA p16n p16n_GOA) [43] Andrew M. P. McDonnell	693918	46.71	100.00
UVP5 UAF_NGA_2018_spring [929] Jess Pretty	0	0.00	0.00
Zooscan UAF test 2 [105] Jess Pretty	7658	0.89	100.00
Zooscan UAF trial [104] Jess Pretty	245	0.00	100.00

For Particle database, upload entire project folder

Notes: Root Folder is the entire project folder – when you have chosen the project, press ‘read Metadata’. This should fill in most of the other blanks on this page

- You can, when importing the project into the particle module, choose to upload already imported vignette project (if you've already imported the Work folder into the Image Database) or 'Create New'.

If importing CTD Data, carefully follow CTD layout requirements (listed in Ecotaxa).
Choose SAVE

Navigating Ecotaxa for Image & Particle Data Upload

1. Contact Marc Picheral for permission to access Ecotaxa & create project

2. Log-in using credentials

Message from the application manager
EcoTaxa now offers Deep Learning features within the usual Random Forest classification !
Videos of the last training (2017/03/16) are available :
• part A : <https://youtu.be/PSO6ZS765tk>
• part B : <https://youtu.be/RaWUqloKk0E>

EcoTaxa is a web application dedicated to the visual exploration and the taxonomic annotation of images that illustrate the beauty of planktonic biodiversity.

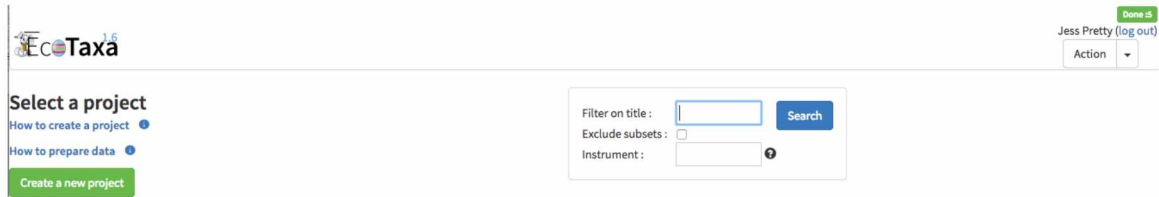
Observatoire Oceanologique de Villefranche-sur-mer Station Biologique de Roscoff Oceanomics Partner University Fund

As a visitor, you have free access to the specimens that have been already identified by taxonomist experts.
You can explore the database by navigating along the UniEuk taxonomic tree which aims at unifying taxonomic names and tree according to reliable and curated molecular phylogenies. It encompasses the whole Eukaryotic and Prokaryotic lineages (Viruses coming soon) that have been molecularly described. Then images can be filtered according to several sample criteria: geographic location, depth, date and time of sampling, and imaging instrument.

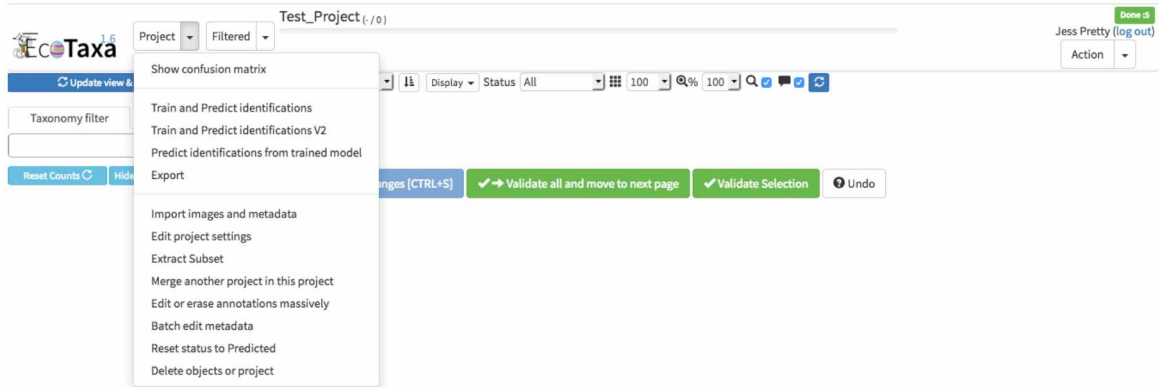
As a scientist, you can contribute to the richness of this image database and/or to the collaborative taxonomic annotation effort. Images are organised in projects which should be consistent in terms of sampling and imaging techniques. We provide tools to support the annotation of large image datasets by supervised machine learning prediction.

Explore Images Contribute to a project

3. Select Contribute to a project



4. Press 'Create a new project' and name according to cruise/date (exact method to be determined)



5. New project screen opens. From dropdown menu next to 'Project', select import images and metadata.

EcoTaxa 3.6 Test_Project Jess Pretty (log out)
Action

Images and TSV file import (Step 1)

[How to create a project](#) | [How to prepare data](#) | [How to import data from zooprocess](#)

Choose a folder or zip file on the server OR Upload folder(s) compressed as a zip file Only for < 100MB zip files.

Contact the project manager to know where and how to upload your data. Once the import is complete, all data folders/files can be safely erased on the server.
Project manager : Jess Pretty (jessica.pretty18@gmail.com)

Skip tsv files that have already been imported
 Skip objects that have already been imported

[Advanced options](#)

Start import Images and TSV files

IMPORTANT NOTE

The maintenance and improvement of EcoTaxa is not free. We would appreciate that you set aside some funds in your next grant to support it. Contact us to estimate what would be both reasonable and useful.

Image Only import

If you have only image and no data file you can use the simple import here.

Start Images only

Re-import and Update Metadata

If you have already loaded your images and you want update your metadata.

Start re-import TSV files to update metadata and data

Import from another database

To import from another Ecotaxa instance in an empty project.

6. Depending on the size of the project, manually upload compressed project folder generated by ImageJ Zooprocess, or if size is too large, choose project from FTP database.

7. Once project is uploaded you are ready to harness Ecotaxa's machine learning power and sort images!

Sorting Images in Ecotaxa

Ecotaxa 1.6

Jess Pretty (log out) Done 15
Action

Select a project
How to create a project
How to prepare data
Create a new project

Filter on title: [] Search
Exclude subsets:
Instrument: [] ?

	Title [ID]	Status	Nb objects	% validated	% classified
Select	Subset of UVP5 UAF (GOA p16n p16n_GOA) created on 2016-04-08 - validated [96] Jess Pretty	Annotate	43319	100.00	100.00
Select	Test_Project [832] Jess Pretty	Annotate	0	0.00	0.00
Select	UVP5 CCELTAR 2016 [156] Tristan Biard	Annotate No Prediction	164571	100.00	100.00
Select	UVP5 Sewardline [62] Andrew M. P. McDonnell	Annotate	31374	0.00	0.00
Select	UVP5 Txs14 [65] Andrew M. P. McDonnell	Annotate	9629	0.00	0.00
Select	UVP5 UAF (GOA p16n p16n_GOA) [43] Andrew M. P. McDonnell	Annotate	693918	46.71	100.00
Select	UVP5 UAF (GOA p16n p16n_GOA) - Equatorial Trial 2 [307] Jess Pretty	Annotate	46309	100.00	100.00
Select	UVP5 UAF (GOA p16n p16n_GOA) - Subset created on 2017-01-20 [279] Jess Pretty	Annotate	21553	57.02	100.00
Select	UVP5 UAF (GOA p16n p16n_GOA) - Subset created on 2017-01-20 [280] Jess Pretty	Annotate	534	100.00	100.00
Select	UVP5 UAF (GOA p16n p16n_GOA) - Subset created on 2017-01-20 [281] Jess Pretty	Annotate	23990	51.17	100.00
Select	UVP5 UAF (GOA p16n p16n_GOA) - Validated by Jess [437] Jess Pretty	Annotate	205515	100.00	100.00
Select	Zooscan UAF test 2 [105] Jess Pretty	Annotate	7658	0.89	100.00
Select	Zooscan UAF trial [104] Jess Pretty	Annotate	245	0.00	100.00

Show projects in which you are not registered

1. Once you are logged into Ecotaxa and have selected ‘Contribute to Project’, select which project you would like to sort images in.

For a new Project, you must first choose to predict the identity of the images using a previously uploaded Learning set. Follow the following steps:

Ecotaxa 1.6

Project: UVP5 Sewardline (0, 0, 31374 / 31374) Filtered

Jess Pretty (log out) Done 15
Action

Update view & Taxonomy filter

▼ Eukaryota (living)

- ▼ Annelida (Metazoa) 9
- Poebolius (Terebellida) 9
- Chaetognatha (Metazoa) 9
- ▼ Cnidaria (Metazoa) 9
- Hydrozoa (Cnidaria) 9
- ▼ Narcomedusae (Trachylina) 9
- Solmundellia bitentaculata 9
- Siphonophorae (Hydrozoalinea) 9

Show confusion matrix
Train and Predict identifications
Train and Predict identifications V2
Predict identifications from trained model
Export

Display: Status: All 100% 100% Q%

None None None None None None None None
None None None None None None None None

a. Select ‘Train and Predict Identifications’

AUTOMATIC CLASSIFICATION : Selection of Learning Set

Learning set is a project containing validated data

USE previous Learning Set: #43 - UVP5 UAF (GOA p16n p16n_GOA)

OR USE another project

ID	Title	Status	Nbr Obj	% Validated	% Classified
Select #96	Subset of UVP5 UAF (GOA p16n p16n_GOA) created on 2016-04-08 - validated	Annotate	43319	100.00	100.00
Select #832	Test_Project	Annotate	0	0.00	0.00
Select #156	UVP5 CCELTER 2016	Annotate No Prediction	164571	100.00	100.00
Select #62	UVP5 Sewardline	Annotate	31374	0.00	0.00
Select #65	UVP5 Txs14	Annotate	9629	0.00	0.00
Select #43	UVP5 UAF (GOA p16n p16n_GOA)	Annotate	693918	46.71	100.00
Select #307	UVP5 UAF (GOA p16n p16n_GOA) - Equatorial Trial 2	Annotate	46309	100.00	100.00
Select #279	UVP5 UAF (GOA p16n p16n_GOA) - Subset created on 2017-01-20	Annotate	21553	57.02	100.00
Select #290	UVP5 UAF (GOA p16n p16n_GOA) - Subset created on 2017-01-20	Annotate	534	100.00	100.00
Select #281	UVP5 UAF (GOA p16n p16n_GOA) - Subset created on 2017-01-20	Annotate	23990	51.17	100.00
Select #437	UVP5 UAF (GOA p16n p16n_GOA) - Validated by Jess	Annotate	205515	100.00	100.00
Select #105	Zooscan UAF test 2	Annotate	7658	0.89	100.00
Select #104	Zooscan UAF trial	Annotate	245	0.00	100.00

b. Select which project you would like to use to base your predictions on. The best choices are those with the majority of objects sorted, and with similar sorting levels to what you are hoping to achieve.

AUTOMATIC CLASSIFICATION : SETTINGS

Classification Method:
START Automatic PREDICTION of IDs

OBJECTS TO PREDICT:

Keep log of previous automatic classification:

Limit number of objects by category from learning set:

- The prediction (automatic classification) will never replace the manual validation
- Default settings for the classification have been validated by experts. User should keep them in most cases
- Classification settings are recorded in EcoTaxa for the next prediction
- Categories selected for the prediction should be correctly validated by expert
- The experience shows that it is often more efficient to automatically classify into a limited number of categories and then validate in detail using more categories

Select Categories with more than Objects

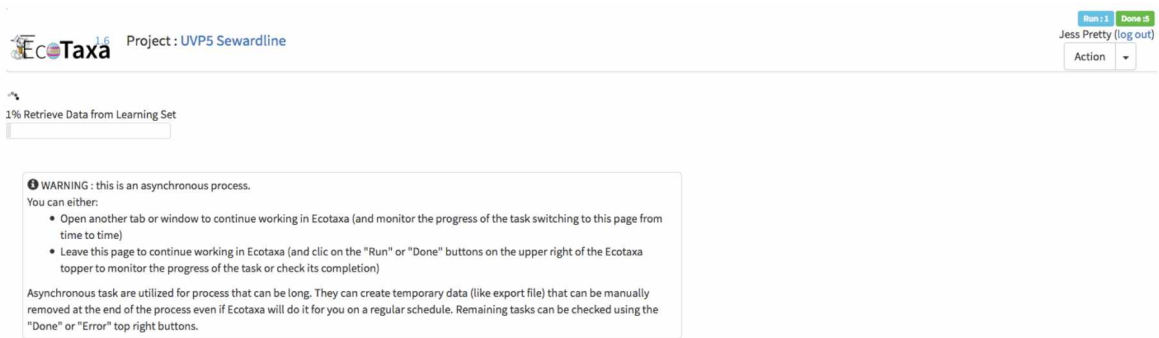
(id) Select	Category	Nbr	%
<input checked="" type="checkbox"/>	detritus (not-living)	94539	57.4 %
<input checked="" type="checkbox"/>	badfocuss (artefact)	33698	20.5 %
<input checked="" type="checkbox"/>	fiber (detritus)	22135	13.5 %
<input checked="" type="checkbox"/>	Aulosphaeridae (Phaeosphaerida)	3782	2.3 %
<input checked="" type="checkbox"/>	like (Copepoda)	2741	1.7 %
<input checked="" type="checkbox"/>	Copepoda (Maxillopoda)	2585	1.6 %
<input checked="" type="checkbox"/>	duplicate (living)	1096	0.7 %
<input checked="" type="checkbox"/>	artefact (not-living)	632	0.4 %
<input checked="" type="checkbox"/>	Eumalacostraca (Malacostraca)	446	0.3 %
<input checked="" type="checkbox"/>	darksphere (othertochek)	430	0.3 %
<input checked="" type="checkbox"/>	Doliolida (Thaliacea)	397	0.2 %
<input checked="" type="checkbox"/>	Rhizaria (Harosia)	278	0.2 %
<input checked="" type="checkbox"/>	solitaryblack (Collodaria)	275	0.2 %
<input checked="" type="checkbox"/>	Acantharea (Retaria)	266	0.2 %
<input checked="" type="checkbox"/>	othertochek (other)	254	0.2 %
<input checked="" type="checkbox"/>	Narcomedusae (Trachylina)	130	0.1 %
<input checked="" type="checkbox"/>	Hydrozoa (Cnidaria)	100	0.1 %
<input checked="" type="checkbox"/>	Siphonophorae (Hydroidolina)	71	0.0 %
<input checked="" type="checkbox"/>	Chaetognatha (Metazoa)	63	0.0 %
<input checked="" type="checkbox"/>	Crustacea (Arthropoda)	61	0.0 %
<input checked="" type="checkbox"/>	colonial (Aulosphaeridae)	59	0.0 %
<input checked="" type="checkbox"/>	spines (Aulacanthidae)	58	0.0 %

Using variables:

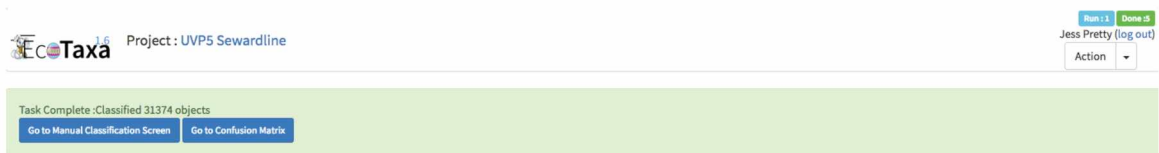
Select ALL / None / Text field content / Uncheck non pertinent variable - Variable help

Select	Object variable	Learning set		Objects to predict	
	Statistics on 50 000 objects	% Pop.	Distinct	ALL	NOT Validated
<input type="checkbox"/>	%area	100	1732	100	100
<input type="checkbox"/>	angle	100	1801	100	100
<input type="checkbox"/>	area	100	956	100	100
<input type="checkbox"/>	area_exc	100	292	100	100
<input type="checkbox"/>	areal	100	685	100	100
<input type="checkbox"/>	bx	100	101	100	100
<input type="checkbox"/>	by	100	96	100	100
<input type="checkbox"/>	cdexc	22	55	22	22
<input type="checkbox"/>	centroids	100	6	100	100
<input type="checkbox"/>	circ	100	980	100	100
<input type="checkbox"/>	circex	100	2533	100	100
<input type="checkbox"/>	compentropy	100	1	100	100
<input type="checkbox"/>	compm1	100	1	100	100
<input type="checkbox"/>	compm2	100	1	100	100
<input type="checkbox"/>	compm3	100	1	100	100
<input type="checkbox"/>	compmean	100	1	100	100
<input type="checkbox"/>	compslope	100	1	100	100
<input type="checkbox"/>	convarea	100	1189	100	100
<input type="checkbox"/>	convarea_area	100	6299	100	100
<input type="checkbox"/>	convperim	100	320	100	100

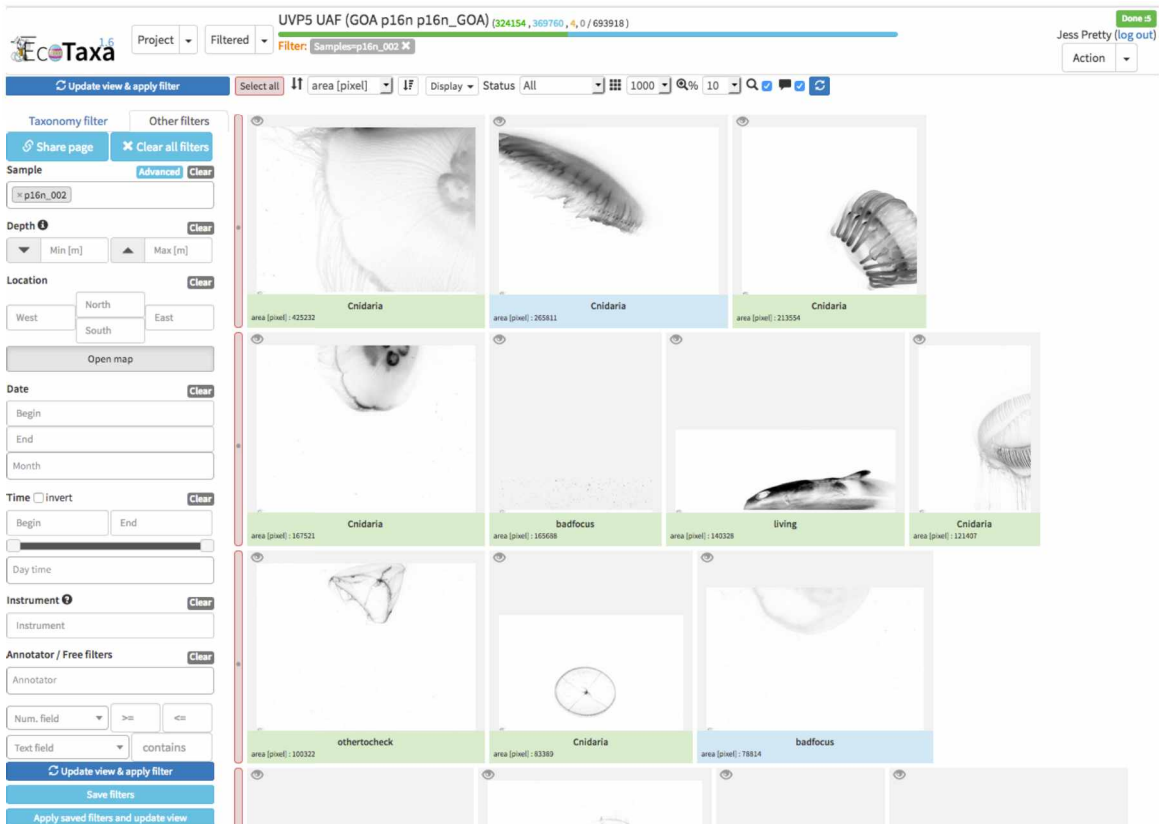
c. This part is very trial and error, so choose variables you would like to sort images in (the lower right portion of the window) and press 'START Automatic PREDICTION of IDs'.



d. This screen pops up while Ecotaxa is predicting your images and shows progress. You can open another window and continue work on another project, but don't exit out of this window.



e. Once this task is complete, you are ready to start validating and sorting images!
- If you don't like the sorting, or want to try a different one then repeat steps above and choose different variables or categories. You can do this multiple times throughout the sorting process. Continue to steps below to sort and validate images.



2. Project opens with last filters used, or entire project opens up if this is your first time opening it – in example above only one station of data is selected (p16n_002).

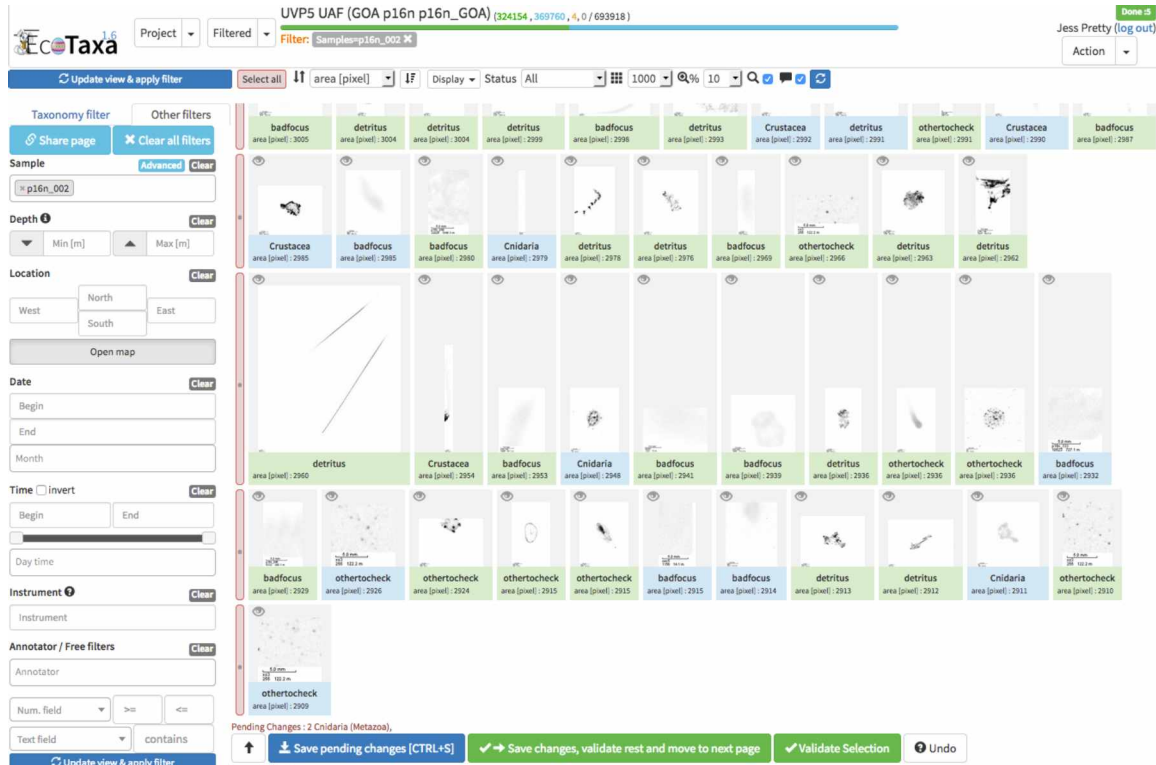
3. Basics of Sorting:

a. Click on image and begin typing name of group you would like to sort into.

To Note: You do not need to click anywhere else, the screen on the upper left-hand corner will automatically appear. Click ‘Enter’ to accept new assignment for image. The name changes to red when you have changed the assignment.

b. You can select multiple images and sort them into the same category by clicking on multiple images – the selected images will be highlighted in red. If you would like to sort them into the same category as was just used, press ‘Command + d’ (or ‘Control + d’ for PC).

c. Continue sorting as many images as desired, changing those that you would like to/need to.

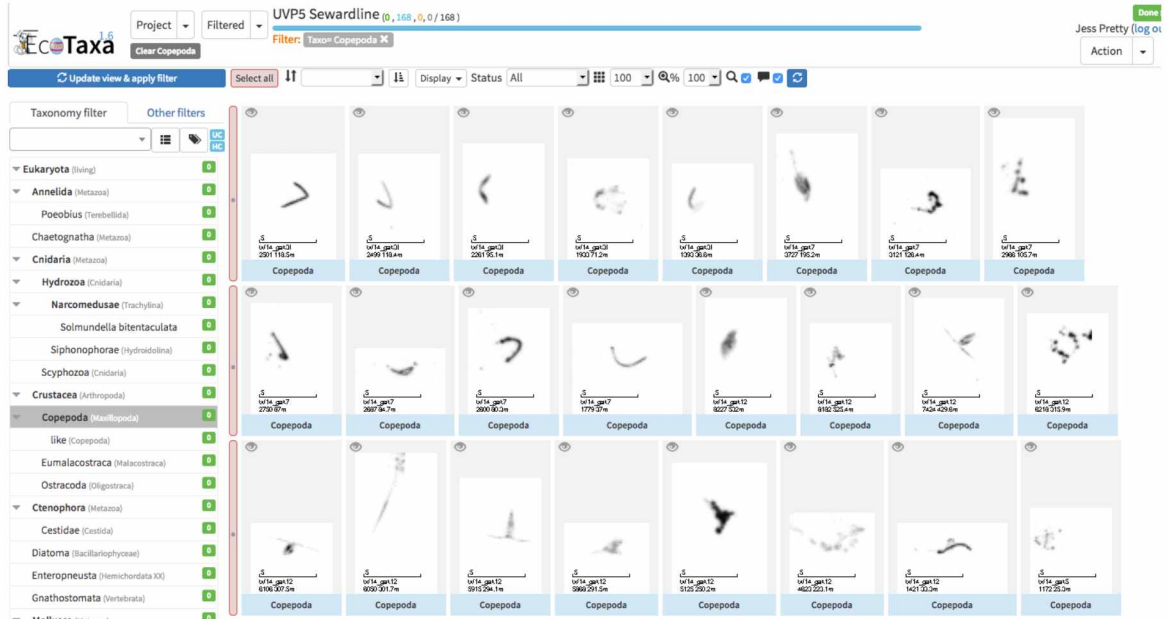


d. When finished with this page, either 'Save pending changes' which will save all changes made and validate those changes, or 'Save changes, validate rest and move to next page'. Be aware of which one you choose to do!



e. You can choose how to sort images in the dropdown menu showing 'area [pixel]'. There are many options here that are useful for different things, so try them out.

f. You can select to zoom in on images (beside the magnifying glass) or zoom out as you see fit, as well as select how many images will be shown per page (shown as '1000' in the above figure).



g. You may choose to only sort one type of predicted image – for example under the taxonomy tab, I chose to only look at images predicted to be copepods in the example above.

Update view & apply filter

Taxonomy filter | Other filters

Share page | Clear all filters

Sample Advanced Clear

Sample

Depth Clear

Min [m] | Max [m]

Location Clear

West | North | East | South

Open map

Date Clear

Begin

End

Month

Time invert Clear

Begin | End

Day time

Instrument Clear

Instrument

Annotator / Free filters Clear

Annotator

Num. field >= <=

Text field contains

Update view & apply filter

Saves filters

h. You may choose to only look at certain stations, regions (based on lat/lon) or depths using the ‘Other Filters’ tabs. Remember to select ‘Update and apply filter’ to apply this to your viewed images.

Project Filtered UVP5 Sewardline (0, 35, 0, 0 / 35)

EcoTaxa Clear Copepoda

Filter: Taxon: Copepoda X | Samples: tf14_gak1, tf14_gak12, tf14_gak5 X

Update view & apply filter | Select all | Display | Status All | 100% | 100% | Action

Jess Pretty (log out)

i. All filters applied will appear at the top of the screen.

After image sorting is finished, your data is ready to be exported and analyzed.

4. Exporting Data from Ecotaxa

EcoTaxa 1.6

Message from the application manager

Welcome to ECOTAXA.

EcoTaxa offers Deep Learning features within the usual Random Forest classification !

Videos of the last training (2017/03/16) are available :

- part A : <https://youtu.be/PSO6ZS765tk>
- part B : <https://youtu.be/RaWUqloKk0E>

Home / Explore

Select Project

Particle Module

Particle projects management

Change Password

Error :10

Jess Pretty (log out)

Action

a. Choose particle module from the home screen, drop down menu

Sample filters :

North

West East

South


Date between Begin and End

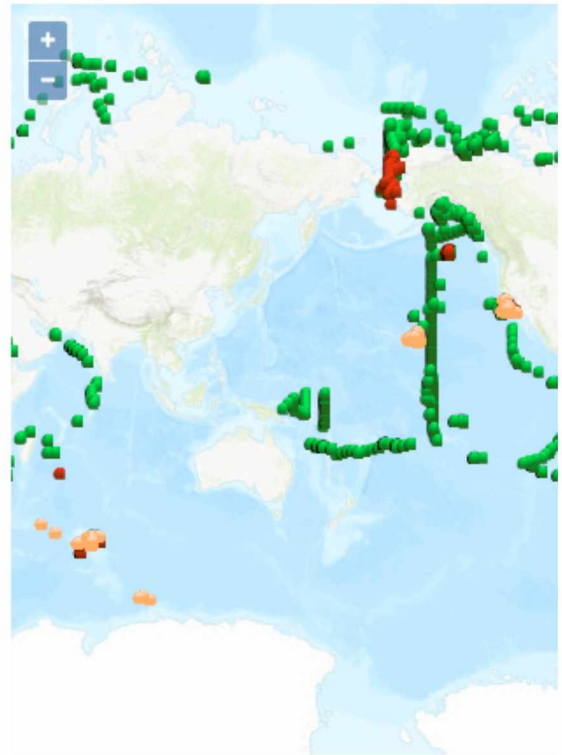
Instrument

Profile type

Ecotaxa Project

Particle Project

Dot color legend 



b. Select the project you would like zooplankton data from under 'Ecotaxa Project' & Press 'Apply Filters' Button




c. Select any extra filters you may want to constrain the data by, and then press 'Export Selection'

Particle sample data export

DOWNLOAD OPTIONS 

Samples filters : filt_proj=43,XScale=1

Samples count : 256

Export format	Options	Description
<input type="radio"/> Reduced data	File format <input type="text" value="ODV"/> Filters :	CTD + PARTICLES abundances and biovolumes sorted in 15 reduced classes at vertical steps of 5m ZOOPLANKTON selected categories at variable vertical steps SUMMARY file (TSV format only) : metadata of exported sample (including pixel size for zooplankton) Apply zooplankton and depth selections from graph - if you do not select any plankton category, the export will return all catégories - if you enable "Sum abundance of children categories", the children counts will be added to the selected category
<input checked="" type="radio"/> Detailed data	File format <input type="text" value="ODV"/>  <input type="checkbox"/> Exclude not living	CTD + PARTICLES abundances and biovolumes sorted in 45 detailed classes at vertical steps of 5m ZOOPLANKTON from all categories and summed in parent categories at vertical steps of 5m SUMMARY file (TSV format only) : metadata of exported sample (including pixel size for zooplankton) Previous screen filter on classification ignored, depth used
<input type="radio"/> RAW	<input type="checkbox"/> Exclude not living <input type="checkbox"/> Include not validated objects	PARTICLES (UVP) : imported « BRU » data compressed and sorted in 1m bins ZOOPLANKTON : annotation and main measurements (pixels) for individual items (possibly excluding not_living items) CTD : as imported SUMMARY file : metadata of exported sample (including pixel size for zooplankton)

In order to ease the transfer of large exported datasets, you can chose to export your files to the Ecotaxa FTP that is utilized to import your data and images.

Do not forget to delete your exported files from the FTP as they will be visible and available for other users.

Ask Ecotaxa managers (piqv@obs-vlfr.fr) if you do not have yet the permissions on this FTP

Save export file on "Exported data" folder on the FTP Area

d. Download data in ODV or TSV format by either direct download locally, or export to FTP site (suggested for large files)



e. If you'd like total zooplankton abundance, or any parameter that is not included in the download, you can edit the tsv/odv file in Excel to add parameters

All screenshots from Ecotaxa database were gathered browsing: <http://ecotaxa.obs-vlfr.fr>

Picheral, M., S. Colin, and J.-O. Irisson. 2017. EcoTaxa, a tool for the taxonomic classification of images. <http://ecotaxa.obs-vlfr.fr>.